Accepted Manuscript

Novel salicylamide derivatives as potent multifunctional agents for the treatment of Alzheimer's disease: design, synthesis and biological evaluation

Qing Song, Yan Li, Zhongcheng Cao, Xiaoming Qiang, Zhenghuai Tan, Yong Deng

Please cite this article as: Q. Song, Y. Li, Z. Cao, X. Qiang, Z. Tan, Y. Deng, Novel salicylamide derivatives as potent multifunctional agents for the treatment of Alzheimer's disease: design, synthesis and biological evaluation, *Bioorganic Chemistry* (2018), doi: https://doi.org/10.1016/j.bioorg.2018.11.022

Novel salicylamide derivatives as potent multifunctional agents for the treatment of Alzheimer's disease: design, synthesis and biological evaluation

Qing Song[a,1], Yan Li[a,1], Zhongcheng Cao[a], Xiaoming Qiang[a], Zhenghuai Tan[b], Yong Deng[a,*]

[a]*Department of Medicinal Chemistry, Key Laboratory of Drug-Targeting and Drug Delivery System of the Education Ministry, Sichuan Engineering Laboratory for Plant-Sourced Drug and Sichuan Research Center for Drug Precision Industrial Technology, West China School of Pharmacy, Sichuan University, Chengdu, 610041, P. R. China*

[b]*Institute of Traditional Chinese Medicine Pharmacology and Toxicology, Sichuan academy of Chinese Medicine Sciences, Chengdu, 610041, P. R. China*

[1] These authors contributed equally to this work.

*Corresponding author.

E-mail: dengyong@scu.edu.cn (Yong Deng)

Abstract

A series of salicylamide derivatives were designed, synthesized and evaluated as multifunctional agents for the treatment of Alzheimer's disease. *In vitro* assays demonstrated that most of the derivatives were selective AChE inhibitors. They showed good inhibitory activities of self- and Cu^{2+}-induced $A\beta_{1-42}$ aggregation, and significant antioxidant activities. Among them, compound **15b** exhibited good inhibitory activity toward *Rat*AChE and *Ee*AChE with IC_{50} value of 10.4 μM and 15.2 μM, respectively. Moreover, **15b** displayed high antioxidant activity (2.46 Trolox equivalents), good self- and Cu^{2+}-induced $A\beta_{1-42}$ aggregation inhibitory potency (42.5% and 31.4% at 25.0 μM, respectively) and moderate disaggregation ability to self- and Cu^{2+}-induced $A\beta_{1-42}$ aggregation fibrils (23.4% and 27.0% at 25 μM, respectively). Furthermore, **15b** also showed biometal chelating abilities, anti-neuroinflammatory ability and BBB permeability. These multifunctional properties indicated compound **15b** was worthy of being chosen for further pharmacokinetics, toxicity and behavioral researches to test its potential for AD treatment.

1. Introduction

Alzheimer's disease (AD) is a neurodegenerative disorder in elderly population and the leading cause of dementia. It is generally characterized by memory loss and cognitive impairments due to the progressive and irreversible damage to the brain [1, 2]. Over 47 million people lived with dementia worldwide in 2015, and it is estimated that this number will increase to more than 131 million by 2050 [3]. AD is one of the most enigmatic and intractable issues in medical science, and there are currently multiple interconnected factors, including β-amyloid (Aβ) deposits, dyshomeostasis of biometals, oxidative stress, neuroinflammation and degeneration of cholinergic neurons in the central nervous system (CNS) [4].

The decreased levels of acetylcholine (ACh) resulting in the learning and memory dysfunctioning, is considered to be a critical determinant of AD pathogenesis [5]. Acetylcholinesterase (AChE) and butyrylcholinesterase (BuChE) are key enzymes that play important roles in cholinergic transmission by hydrolyzing the ACh. AChE was validated as a therapeutic target to increase cholinergic levels, and AChE inhibitors are effective in temporarily restoring cholinergic function. But BuChE is mainly distributed in the peripheral areas, and the inhibition of BuChE may bring certain peripheral side effects [6]. Therefore, the development of AChE inhibitors may be a more rational therapeutic strategy for AD.

The increased production and accumulation of Aβ oligomer in brain also plays a pivotal role in AD pathogenesis. The Aβ peptide is generated after enzymatic cleavage of the amyloid precursor protein (APP) [7]. APP follows two distinct cleavage pathways. In the non-amyloidogenic one, APP is first cleaved by α- and γ-secretase to form interceptive A$\beta_{17-40/42}$ peptides or Aβ_{1-16} peptide. In the amyloidogenic one, which occurs to a minor extent, APP is cleaved consecutively by β- and γ-secretases leading to the formation of full-length Aβ peptides (mainly A$\beta_{1-40/42}$) [8]. Although Aβ_{1-40} presents in larger amounts in brain, Aβ_{1-42} displays lower solubility and higher tendency to aggregate, leading to the formation of oligomers species that are reorganized into protofibrils and fibrils, found in amyloid plaques [9]. Therefore, preventing the Aβ_{1-42} aggregation in the brain may be a potent therapeutic strategy for AD.

Some evidence suggests that oxidative stress plays an important role in the pathogenesis of AD [10]. Generally, reactive oxygen species (ROS) are kept at a low level but not fully eliminated.

Accumulation of too high levels of ROS is dangerous and defined as oxidative stress [11]. Oxidative stress occurs early in the initiation of AD, and is associated with the presence of Aβ [12, 13]. Moreover, it has been proposed that oxidative stress acts as aberrant signaling pathways, resulting in progressive damage to the neuronal network [14]. In turn, both toxic Aβ and excessive neuronal excitation can induce ROS production [15]. The vicious cycle makes things worse. According to these, molecules with antioxidant abilitiy may be a good therapy for AD.

In recent years, with the emphasis on the inflammatory mechanism of AD, it's suggested that neuroinflammation may be another important pathogenesis of AD [16]. Epidemiological studies have identified a link between chronic use of NSAIDs and reduced risk of AD [17]. They showed the protective effect of the long-term use of NSAIDs in AD patients, reducing or delaying the development of the disease, although the mechanism of this protective effect is still unclear. Neuroinflammation of AD is mainly manifested by activation of microglial cells in the brain. Microglia cells are widely distributed in brain, spinal cord, retina and optic nerve, but mainly in the hippocampus and substantia nigra [18]. Activated microglia can produce proinflammatory cytokines like TNF-α, IL-1, IL-6 and chemokines. These inflammatory factors will promote the formation of chronic neuroinflammation, lead to neuron death, and aggravate neurodegenerative lesions [19-21]. Therefore, the use of NSAIDs to relieve neuroinflammation has brought hope to patients with AD.

Salicylic acid (SA) has been widely used for years as an anti-inflammatory drug. As the discovery and further studies of the effect of neuroinflammation on AD, biological activities of SA and its derivatives drew people's concern. The studies indicated that SA had certain anticholinesterase activity (IC$_{50}$ = 346.0 μM) [22]. In addition, salicylic acid derivatives could inhibit LPS-induced activation of microglia cells and astrocytes, and reduce the production of relevant pro-inflammatory factors [23]. *In vivo* experiments, salicylic acid derivatives could significantly improve the cognitive and memory function in a transgenic mouse model of AD [24]. The above research results showed that SA can be used as a leading compound to design new anti-AD drugs.

Because of the complex etiology of AD, the single-target directed drugs which have reached clinical trials have failed. Recently, more researches in AD have been paid attention to the development of "multi-target-directed ligands" (MTDLs), by which new scaffolds aiming at two or more disease targets are designed. Based on previous research of our group, the introduction of the alkylbenzylamine group to chromone significantly increased the inhibitory activity of AChE, and the

chromone derivative (**II**) is multifunctional agent for AD treatment [25]. But the molecular weights (MW) of chromone derivatives are a little high. MW is one of the most important physicochemical properties that affect membrane permeability, for its reduction often has coincidental beneficial effects on other parameters, such as rotatable bonds, PSA, and cLogP [26]. Studies showed CNS drugs tend to be smaller than non-CNS therapeutics, and the mean MW derived from an analysis of marketed CNS drugs is 310, which offers useful guidance when defining a desirable CNS candidate [27]. Lipinski and Levin *et al.* have also suggested that MW should be kept below 400 [28, 29]. Therefore we replaced chromone nucleus with salicylic to reduce their MW for better membrane permeability. According to these, we designed a series of *N*-alkylbenzylamine salicylamide derivatives (**Figure 1**) by using multi-target-directed drug design strategy to combine salicylic acid with appropriate secondary amines using carbon spacers of different lengths. Furthermore, we found that the inhibitory activity of chromone derivatives toward AChE increased a little and even began to decrease when the linker was up to 6. So based on this trend of structure-activity relationship, we designed the salicylamide derivatives with the longest linker of 6. These new molecules may simultaneously possess membrane permeability, AChE inhibition, antioxidative and metal chelating effects, anti-inflammatory and anti-*β*-amyloid aggregation properties.
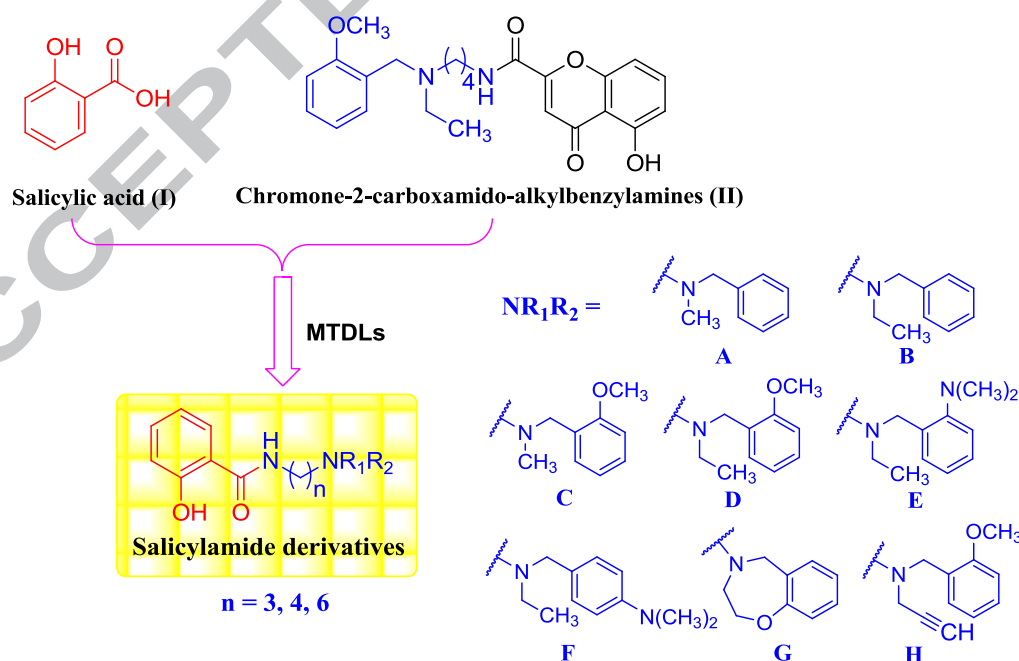

Figure 1. Design strategy of the *N*-alkylbenzylamine salicylamide derivatives.

2. Results and discussion

2.1. Chemistry

The synthetic pathways of target derivatives were summarized in **Scheme 1**. Compound **2** was synthesized from phtalimide (**1**) reacted with KOH. Then compound **2 was** reacted with excessive amounts of 1,3-dibromopropane, 1,4-dibromobutane or 1,6-dibromohexane in the presence of PEG-400 in acetone to obtain intermediates **3-5** [30]. In turn, these intermediates were reacted with the corresponding secondary amines **6a-h** [25], to provide the intermediates **7-9** respectively. The latter were reacted with hydrazine hydrate to obtain the key primary amine intermediates **10-12** [31]. Finally, salicylic acid (**I**) was condensed with the corresponding primary amine **10-12** in the presence of 1-(3-dimethylaminopropyl)-3-ethyl carbon imine hydrochloride (EDCI) in THF to provide the *N*-alkylbenzylamine salicylamide derivatives **13-15**. All of the target compounds were characterized by ^{1}H NMR and ESI-MS, and most of them were further characterized by ^{13}C NMR. The purity of all target compounds was determined by high-performance liquid chromatography (HPLC) analysis to be over 97.0 %.
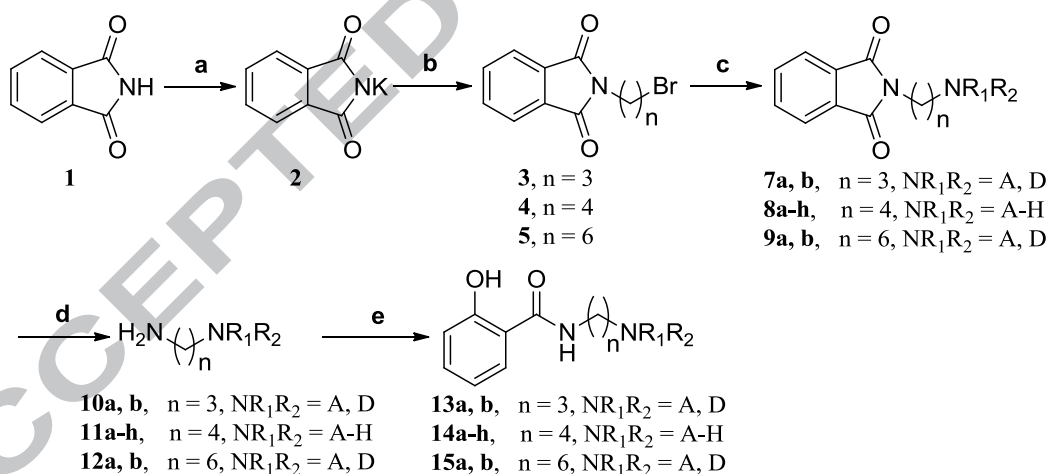
Scheme 1. Synthesis of salicylamide derivatives **13-15**. *Reagents and conditions:* (a) KOH, EtOH, reflux; (b) Br(CH$_2$)$_n$Br, PEG400, acetone, reflux for 5-8 h; (c) R$_1$R$_2$NH (**6a-h**), K$_2$CO$_3$, CH$_3$CN, reflux for 6-8 h; (d) H$_2$NNH$_2$•H$_2$O, EtOH, reflux for 6 h; (e) Salicylic acid (**I**), EDCI, THF, r.t., overnight.

2.2. Pharmacology
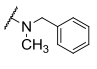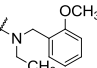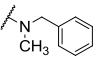
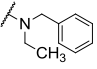### 2.2.1. Evaluation of AChE and BuChE inhibitory activities
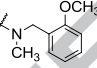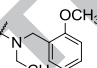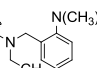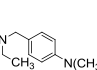
All the synthesized salicylamide derivatives were evaluated for their inhibitory activities toward AChE and BuChE *in vitro* according to modified Ellman's method [32, 33]. AChE activity was measured from both rat cortex homogenate and *Electrophorus electricus*, and BuChE activity was measured from rat serum. Rivastigmine and donepezil were used as reference compounds. The ChE inhibitory results are summarized in **Table 1**.

As shown in **Table 1**, salicylamide derivatives (**13-15**) showed different AChE inhibitory activities with IC_{50} values ranging from 10 μM to 200 μM. The structure-activity relationship analysis showed that the AChE inhibitory activity of the compound was closely related to its methylene side chain length and terminal benzylamine species. The conversion of these two factors can improve the interaction between the molecule and the CAS and PAS sites of the enzyme. From the results of compounds **14a-h**, fixing the side chain length, we could find benzylamine moiety had a large effect on the activity. In general, compounds having benzylamine moieties with *N*-ethyl (**14b**, **14d** and **14e**) or *N*-propargyl (**14h**) substitutions were more active than those with *N*-methyl substitution (**14a** and **14c**). Compounds with 2-methoxybenzylamine (**14c-d** and **14h**) or 2-dimethylaminobenzylamine (**14e**) were more active than the compounds (**14a-b**) with unsubstituted benzylamine moiety. In conclusion, the (2-methoxybenzyl) ethylamine moiety was optimal for the inhibition of AChE. Then, we found the introduction of (4-dimethylaminobenzyl) ethylamine and the benzoxazepine moiety (**14f** and **14g**) did not significantly increase or even decrease the activity. Especially, compound **14g** almost had no AChE inhibitory activity, which indicated that rigid structure of the terminal benzylamine may be not conducive to its interaction with the enzyme activity center. In addition, the activities of compounds **15a-b** (n = 6) were significantly higher than those of corresponding **13a-b** (n =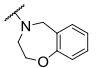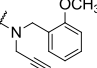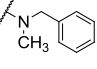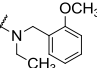 3), **14a** and **14d** (n = 4). Therefore, a 6-methylene linker was beneficial for AChE inhibitory activity. Among the tested derivatives, **15b** exhibited the most potent inhibitory activity for both *Rat*AChE and *Ee*AChE (IC_{50} = 10.4 μM and 15.2 μM, respectively), which was more excellent than rivastigmine (IC_{50} = 37.1 μM and 23.2 μM, respectively) but less than donepezil (IC_{50} = 0.015 μM and 0.021μM, respectively) under our experimental condition. Compared with chromone derivative (**II**) (IC_{50} = 0.07 μM and 0.55 μM, respectively) [25], the activity of compound **15b** is relatively lower. Camparing the molecular docking results of these two compounds, a strong hydrogen bond was observed between the 4-carbonyl group at the chromone moiety and Tyr121, which may contribute to the better inhibitory

activity of chromone derivative (**II**) toward AChE.

All salicylamide derivatives were inactive or weak on BuChE inhibitory activity. These results showed the target compounds were potent AChE inhibitors with high selectivity. It may be beneficial to diminish peripheral cholinergic side effects and provide lower toxicity. Based on the above results, we selected **15b** for kinetic analysis of AChE inhibition.

Table 1. *In vitro* inhibition of AChE and BuChE and oxygen radical absorbance capacity (ORAC, Trolox Equivalents) by salicylamide derivatives (**13-15**) and reference compounds.

Compd.	n	NR$_1$R$_2$	IC$_{50}$ (μM) $\pm$ SD[a]			ORAC[e]
			*Rat*AChE[b]	*Rat*BuChE[c]	*Ee*AChE[d]	
13a	3	(N–CH$_3$, benzyl)	200.0 $\pm$ 5.12	175.0 $\pm$ 6.06	>200	2.00 $\pm$ 0.05
13b	3	(N–CH$_3$, OCH$_3$-benzyl)	68.5 $\pm$ 1.22	>200	>200	2.80 $\pm$ 0.02
14a	4	(N–CH$_3$, benzyl)	190.0 $\pm$ 3.48	177.0 $\pm$ 7.63	>200	2.55 $\pm$ 0.07
14b	4	(N–CH$_3$, benzyl)	160.0 $\pm$ 2.57	>200	>200	2.32 $\pm$ 0.03
14c	4	(N–CH$_3$, OCH$_3$-benzyl)	103.0 $\pm$ 1.18	>200	118.0 $\pm$ 2.45	2.90 $\pm$ 0.07
14d	4	(N–CH$_3$, OCH$_3$-benzyl)	31.4 $\pm$ 0.73	>200	68.2 $\pm$ 0.99	1.74 $\pm$ 0.05
14e	4	(N–CH$_3$, N(CH$_3$)$_2$-benzyl)	65.0 $\pm$ 2.90	98.5 $\pm$ 2.77	>200	2.49 $\pm$ 0.09
14f	4	(N–CH$_3$, N(CH$_3$)$_2$-benzyl)	170.0 $\pm$ 3.39	>200	>200	2.91 $\pm$ 0.03
14g	4	(benzoxazepine)	n.a.[f]	134.0 $\pm$ 4.82	>200	2.82 $\pm$ 0.06
14h	4	(N–propargyl, OCH$_3$-benzyl)	71.1 $\pm$ 4.22	>200	>200	1.24 $\pm$ 0.06
15a	6	(N–CH$_3$, benzyl)	21.2 $\pm$ 1.10	191.0 $\pm$ 12.70	17.7 $\pm$ 0.20	2.20 $\pm$ 0.04
15b	6	(N–CH$_3$, OCH$_3$-benzyl)	10.4 $\pm$ 0.478	106.0 $\pm$ 5.01	15.2 $\pm$ 0.33	2.46 $\pm$ 0.03
Rivastigmine	—	—	37.1 $\pm$ 1.22	9.87 $\pm$ 0.23	23.2 $\pm$ 0.44	n.t.[g]
Donepezil	—	—	0.015 $\pm$ 0.002	20.7 $\pm$ 0.36	0.021 $\pm$ 0.003	n.t.[g]

[a] IC$_{50}$ values represent the concentration of inhibitor required to decrease enzyme activity by 50% and are the mean of 3 independent experiments, each performed in triplicate (SD = standard deviation).

[b] From 5% rat cortex homogenate.

[c] BuChE from rat serum and tested compounds were used at 50 μM.

[d] From *Electrophorus electricus*.

[e] The mean ± SD of the three independent experiments. The data are expressed as μM of Trolox equiv/μM of tested compound.

[f] n.a. = no active. Compounds defined "no active" means that percent inhibition is less than 5.0% at a concentration of 50 μM in the assay conditions.

[g] n.t. = not tested.

2.2.2. Kinetic study for the inhibition of AChE

To gain further insight into the inhibitory mechanism of this family of compounds, **15b**, the most potent AChE inhibitor among these compounds, was chosen for a kinetic study using *Ee*AChE [34]. The graphical presentation of the reciprocal Lineweaver-Burk plots (**Figure 2**) showed that with the concentrations of **15b** increasing, both the slopes (decreased V$_{max}$) and intercepts (higher K$_m$) were increased. This pattern indicated a mixed-type inhibitory behavior for **15b** as the consequence of binding to both the CAS and PAS of AChE.
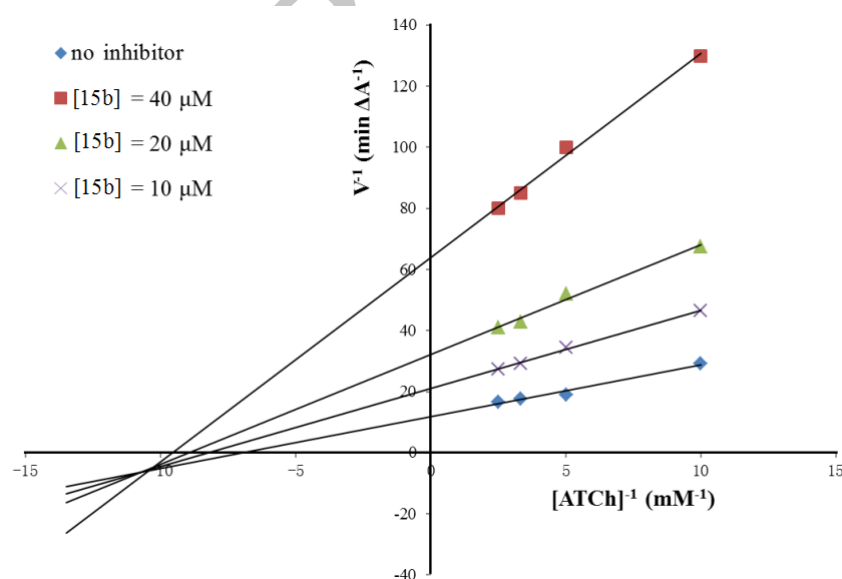
Figure 2. Kinetic study on the mechanism of *Ee*AChE inhibition by compound **15b**. Overlaid Lineweaver-Burk reciprocal plots of AChE initial velocity at increasing substrate concentration (0.1-0.4 mM) in the absence and presence of **15b** are shown. Lines were derived from a weighted least-squares analysis of data points.

2.2.3. Molecular modeling study

To explore the possible interacting mode of the salicylamide derivatives with *Tc*AChE (PDB code: *1EVE*), a molecular modeling study was performed using the docking program, AutoDock 4.2 package with Discovery Studio 2.5 [35]. The results showed in **Figure 3** indicated that compound **15b** occupied the entire enzymatic CAS, the mid-gorge sites and the PAS, and binds simultaneously to both the catalytic site and peripheral site. In the *Tc*AChE-**15b** complex, the secondary amine moiety of the amide of **15b** interacted with residue Phe331 via hydrogen bond interaction. In addition, the *N*-(2-methoxybenzyl) ethylamine moiety in the side chain of **15b** was observed to bind to the CAS via parallel π-π interactions with Trp84 and exhibited a potential hydrophobic interaction with residues Asp72, Phe330, His440 and Gly441. Furthermore, the conformation formed by the folding methylene side chain and the salicylamide ring in the gorge allowed them to interact with the residues Gly118, Tyr121, Trp279, Ser286, Ile287, Phe288, Phe290, Phe331, Tyr334 and Gly335 via the hydrophobic interaction. The docking results, consistent with the kinetic analysis, indicated that compound **15b** could simultaneously bind to the CAS and PAS of AChE, and explained its high AChE inhibitory activities.

Figure 3. Representation of compound **15b** (grey stick) interacting with residues in the binding site

of *Tc*AChE (PDB code: *1EVE*), highlighting the protein residues that participate in the main interactions with the inhibitor.
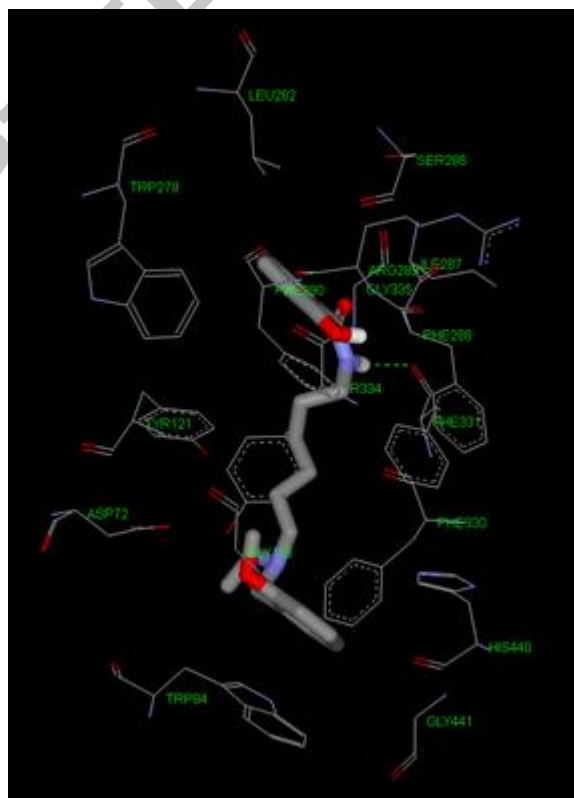
2.2.4. Antioxidant activity assay

The antioxidant activities of the salicylamide derivatives were evaluated by the well-established ORAC-FL method (oxygen radical absorbance capacity by fluorescein) [36] and the results were shown in **Table 1**. The activities of tested compounds to scavenge radicals were expressed as Trolox (a water-soluble vitamin E analog) equivalent. And their relative activity at concentration of 5 μM was compared with the highly potent compound Trolox. All the tested compounds displayed high peroxyl radical absorbance capacities, ranging from 1.24 to 2.91-fold of Trolox. Among them, compound **14f** exhibited the strongest free radical scavenging activity with ORAC-FL value of 2.91 Trolox equivalents due to the introduction of (4-dimethylaminobenzyl) ethylamino moiety. However, the introduction of propyl (Compound **14h**) reduced the activity of the compound with an ORAC-FL value of 1.24 Trolox equivalents. Representative compound **15b** showed good antioxidant activity with an ORAC-FL value of 2.46 Trolox equivalents, which was significantly better than chromone derivative (**II**) (0.83 Trolox equivalents) [25].

2.2.5. Metal-chelating studies

The chelating ability of compound **15b** with biometals: Cu^{2+}, Zn^{2+}, Fe^{2+} and Al^{3+}, was evaluated by UV-visual spectrometry [37, 38], and the results were shown in **Figure 4A**. We could find the UV-Vis spectra of **15b** changed significantly after the addition of $CuCl_2$ and $AlCl_3$, with a shoulder peak appearing at 342 nm and 330 nm, respectively, which indicated the formation of **15b**-Cu^{2+} and **15b**-Al^{3+} complexes. In addition, the absorption increased significantly when $CuCl_2$, $FeSO_4$ and $AlCl_3$ were added, indicating a possible interaction between the compound **15b** and these biometals. However, the addition of $ZnCl_2$ to **15b** solution showed no significant change in the spectra.

To further determine the stoichiometry of **15b**-Cu^{2+} complex, molar ratio method was used by preparing the methanol solutions of compound **15b** with increasing amounts of $CuCl_2$. The UV spectra were used to obtain the absorbance of the **15b** complex and different concentrations of $CuCl_2$ at 342 nm. As indicated in **Figure 4B**, the absorbance linearly increased initially and then plateaued. The two straight lines intersected at a mole fraction of 0.97, revealing a 1:1 stoichiometry for **15b**-Cu^{2+} complex.
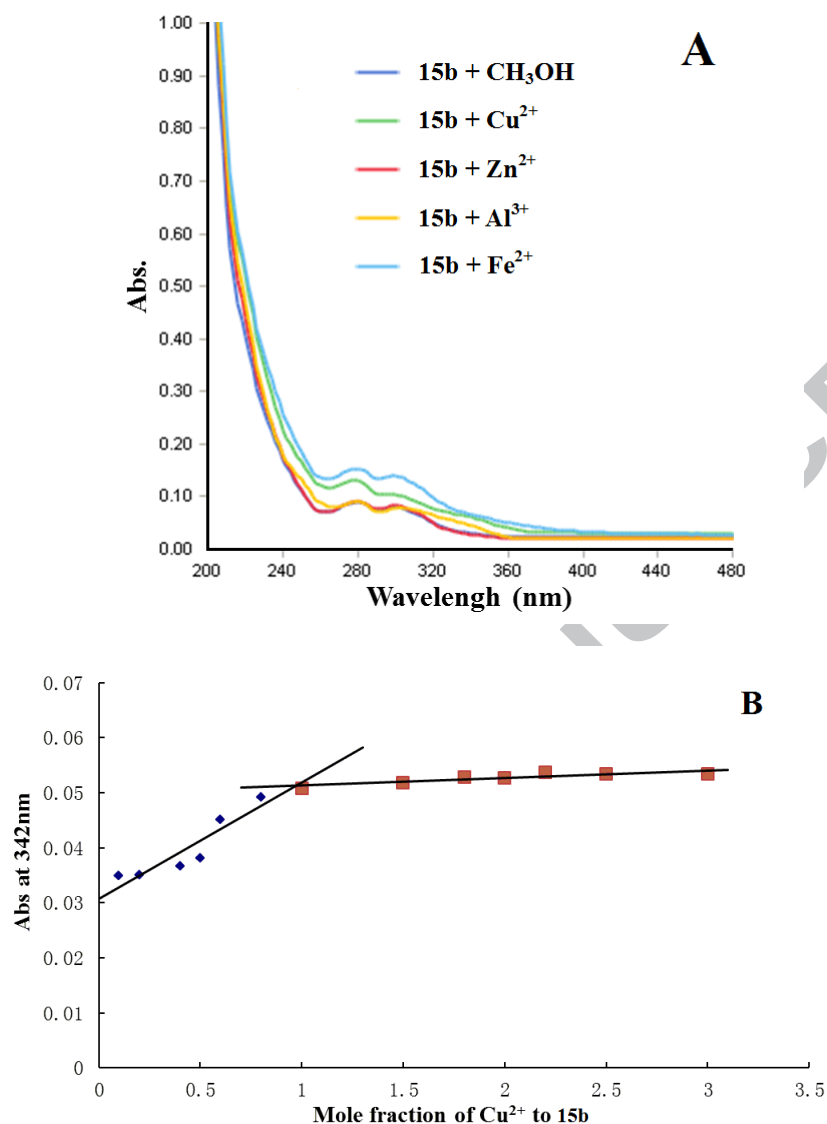
Figure 4. (**A**) UV spectra of compound **15b** (37.5 μM in methanol) alone or in the presence of CuCl$_2$, ZnCl$_2$, AlCl$_3$ or FeSO$_4$ (37.5 μM, in methanol). (**B**) Determination of the stoichiometry of complex-Cu^{2+} by using the molar ratio method titrating the methanol solution of compound **15b** with ascending amounts of CuCl$_2$. The final concentration of tested compound was 37.5 μM, and the final concentration of Cu^{2+} ranged from 3.75 to 150 μM.

2.2.6. Inhibition of self- and Cu^{2+}-induced Aβ$_{1-42}$ aggregation

The activities of the target compounds on inhibiting self- and Cu^{2+}-induced Aβ$_{1-42}$ aggregation were evaluated by a thioflavin T (ThT) fluorescence assay, with curcumin as a reference compound [39-42]. The results summarized in **Table 2** indicated that all the target compounds showed moderate to good inhibitory activities of self-induced Aβ$_{1-42}$ aggregation with inhibition ratios ranging from

25.1% to 45.1% at 25 μM, compared with that of curcumin (40.2% at 25 μM). However, most of compounds showed poor inhibitory activity against Cu^{2+}-induced $A\beta_{1-42}$ aggregation with the percentage ranging from 8.6% to 31.4%. Furthermore, the representative compound **15b** exhibited moderate inhibitory potency of self- and Cu^{2+}-induced $A\beta_{1-42}$ aggregation with the percentage of 42.5% and 31.4%, respectively, which had relatively weaker activities compared with chromone derivative (**II**) (59.2% and 48.3%, respectively) [25]. For the inhibition of self-induced $A\beta_{1-42}$ aggregation, compound **14d** (n = 4) exhibited the highest inhibitory activity with inhibition ratios of 45.1%. Interestingly, compound **13b** (37.1%) and **15b** (42.5%) respectively exhibited the highest inhibitory activity among the derivatives with a 3-methylene linker and 6-methylene linker. It showed an *N*-(2-methoxybenzyl) ethylamine group on the terminal side of carbon chain among the compounds **13b**, **14d** and **15b** may be optimal for the inhibition of self-induced $A\beta_{1-42}$ aggregation, which was same as the conclusion resulting from the AChE inhibition assay. As for the Cu^{2+}-induced $A\beta_{1-42}$ aggregation, the most potent inhibitor was **15b**. But the length of the alkyl chain and terminal benzylamine species had no significant effect against Cu^{2+}-induced $A\beta_{1-42}$ aggregation.

Table 2. *In vitro* inhibition of self- and Cu^{2+}-induced $A\beta_{1-42}$ aggregation by salicylamide derivatives and reference compound.

Compd.	n	% Inhibition of $A\beta_{1-42}$ aggregation[a]		% Disaggregation of $A\beta_{1-42}$ aggregation[e]	
		Self-induced[b,d]	Cu^{2+}-induced[c,d]	Self-induced[f,d]	Cu^{2+}-induced[g,d]
13a	3	34.0 ± 1.0	11.5 ± 0.2	n.t.[h]	n.t.[h]
13b	3	37.1 ± 0.9	14.1 ± 0.3	25.4 ± 0.8	40.5 ± 1.2
14a	4	32.4 ± 1.2	22.6 ± 0.7	n.t.[h]	n.t.[h]
14b	4	36.2 ± 1.3	15.6 ± 0.9	n.t.[h]	n.t.[h]
14c	4	31.6 ± 1.1	13.8 ± 0.8	n.t.[h]	n.t.[h]
14d	4	45.1 ± 2.0	10.9 ± 0.1	29.4 ± 0.6	35.6 ± 1.3
14e	4	25.1 ± 0.6	9.8 ± 0.3	n.t.[h]	n.t.[h]
14f	4	29.1 ± 0.8	11.1 ± 0.5	n.t.[h]	n.t.[h]
14g	4	26.2 ± 0.6	23.6 ± 1.3	n.t.[h]	n.t.[h]
14h	4	25.3 ± 1.0	8.6 ± 0.1	n.t.[h]	n.t.[h]
15a	6	33.7 ± 1.4	17.6 ± 0.9	n.t.[h]	n.t.[h]
15b	6	42.5 ± 0.9	31.4 ± 1.0	23.4 ± 0.6	27.0 ± 0.9
Curcumin	—	40.2 ± 0.9	66.0 ± 1.3	n.t.[h]	54.7 ± 1.0

[a] For inhibition of Aβ aggregation, the thioflavin-T fluorescence method was used.

[b] Inhibition of self-induced A$\beta_{1\text{-}42}$ aggregation (25 μM) by tested inhibitors at 25 μM.

[c] Inhibition of Cu^{2+}-induced A$\beta_{1\text{-}42}$ aggregation. The concentration of tested compounds and Cu^{2+} were 25 μM.

[d] The mean ± SD of the three independent experiments.

[e] For disaggregation of Aβ aggregation fibrils, the thioflavin-T fluorescence method was used.

[f] For disaggregation of self-induced A$\beta_{1\text{-}42}$ aggregation fibrils, the concentration of tested compounds and A$\beta_{1\text{-}42}$ were 25 μM.

[g] For disaggregation of Cu^{2+}-induced A$\beta_{1\text{-}42}$ aggregation fibrils, the concentration of tested compounds and Cu^{2+} were 25 μM.

[h] n.t. = not tested.

2.2.7. Effect on the disaggregation of A$\beta_{1\text{-}42}$ aggregation fibrils

We selected some relatively high active salicylamide derivatives (**13b**, **14d** and **15b**) to test their disaggregation ability to the formed Aβ fibers. The results were summarized in **Table 2**. Compounds **13b**, **14d** and **15b** manifested the disaggregation potency of self- induced A$\beta_{1\text{-}42}$ aggregation fibrils with the percentage of 25.4%, 29.4% and 23.4%, respectively. As for those of disaggregation of Cu^{2+}-induced A$\beta_{1\text{-}42}$ aggregation fibril, their disaggregation ratios were 40.5%, 35.6% and 27.0%, respectively. It revealed that these compounds could not only inhibit the aggregation of A$\beta_{1\text{-}42}$, but also depolymerize the A$\beta_{1\text{-}42}$ aggregation fibrils, with the potency of inhibiting and eliminating Aβ plaques in AD brains.

2.2.8. In vitro blood-brain barrier permeation assay

For the drug targeting on central nervous system, it is an important prerequisite for its efficacy to penetrate the blood-brain barrier (BBB). A parallel artificial membrane permeation assay of the blood-brain barrier (PAMPA-BBB) was performed to determine the BBB penetration of the target compounds [43]. First, the experimental permeabilities of 11 commercial drugs were compared with reported values (**Table S1**, Supplementary Material). A plot of experimental data versus bibliographic values produced a good linear correlation: P_e (exp.) = 0.9163 × P_e (bibl.) − 0.2247 (R^2 = 0.9558) (**Figure S1**, Supplementary Material). Combined with the evaluation conditions established by Di *et al.* [44] for BBB permeation, we determined that compounds with P_e values above 3.44 × 10^{-6} cm/s could cross the BBB (**Table S2**, Supplementary Material). The representative compound **15b** was selected for this assay. As the result was shown in **Table 3**, compound **15b** exhibited good BBB permeabilities and would be able to reach the therapeutic targets in central

nervous system (CNS).

Table 3. Permeability results P_e ($\times 10^{-6}$ cm/s) from the PAMPA-BBB assay for **15b** with its predicted penetration into the CNS.

Compd.[a]	P_e ($\times 10^{-6}$ cm/s)[b]	Prediction
15b	6.27 ± 0.12	CNS +

[a] Compound **15b** was dissolved in DMSO at 5 mg/mL and diluted with PBS/EtOH (70:30). The final concentration of each compound was 100 μg/mL.

[b] Data are the mean $\pm$ SD of three independent experiments.

### 2.2.9 *In vitro anti-neuroinflammatory activity assay*

Neuroinflammation in AD is mainly characterized by the activation of microglia in the brain and the release of multiple proinflammatory cytokines. To evaluate the anti-neuroinflammatory activity of the target compounds, representative compound **15b** was tested with the inflammatory BV-2 microglial stimulated by lipopolysaccharide (LPS). Flurbiprofen and salicylic acid were used as reference compound. *In vitro* neurocytotoxicity, inhibition of LPS induced NO and TNF-α production were investigated [45-48].

The *in vitro* cytotoxicity assay was carried out by the MTT method. As the results shown in **Figure 5**, whether adding LPS (0.1 μg/mL) or not, cell viability did almost not change after treatment with various concentrations of all the compounds (0.5, 2.5 and 10.0 μM). It indicated compound **15b** was not toxic toward the BV-2 cell at concentrations below 10 μM, and LPS (0.1 μg/mL) could not alter cell viability also.

Inhibition of LPS-induced NO production was measured by using Griess reaction method. First, we examined the effect of compounds themselves on NO release from BV-2 cells without LPS. As shown in **Figure 6**, NO release volume didn't change a lot compared with the control group, so compounds had no effect on it. Then in LPS-treated cells, we observed a massive induction of NO production, which was significantly reduced by treatment with **15b** in a dose-dependent manner. **15b** displayed NO inhibitory activity with the respective percentages of 13.3%, 30.0% and 55.0% when the cells were treated with 0.5, 2.5 and 10.0 μM, which was much better than flurbiprofen (11.8% and 23.0% when the cells were treated with 2.5 and 10.0 μM) and **SA** (10.0% and 18.5% when the cells were treated with 2.5 and 10.0 μM).

15

Inhibition of LPS-induced TNF-α production was measured by the enzyme-linked immunosorbent assay (ELISA). The results were shown in **Figure 7**. First we could also find that **15b** had no effect on TNF-α production without LPS up to the concentration of 10 μM. Then in LPS-treated cells, **15b** showed moderate inhibitory activities on LPS-induced TNF-α production with the respective inhibition ratios of 13.5%, 27.1% and 45.3% when the cells were treated with 0.5, 2.5 and 10.0 μM, which was still much better than flurbiprofen (9.6% and 30.3% when the cells were treated with 2.5 and 10.0 μM) and **SA** (7.6% and 20.6% when the cells were treated with 2.5 and 10.0 μM).

The above results indicate that the introduction of the alkylbenzylamine group to salicylic acid can improve its anti-inflammatory activity, which may partly due to the enhancement of its lipid solubility. All these suggest that **15b** is a promising antiinflammatory and neuroprotective agent.
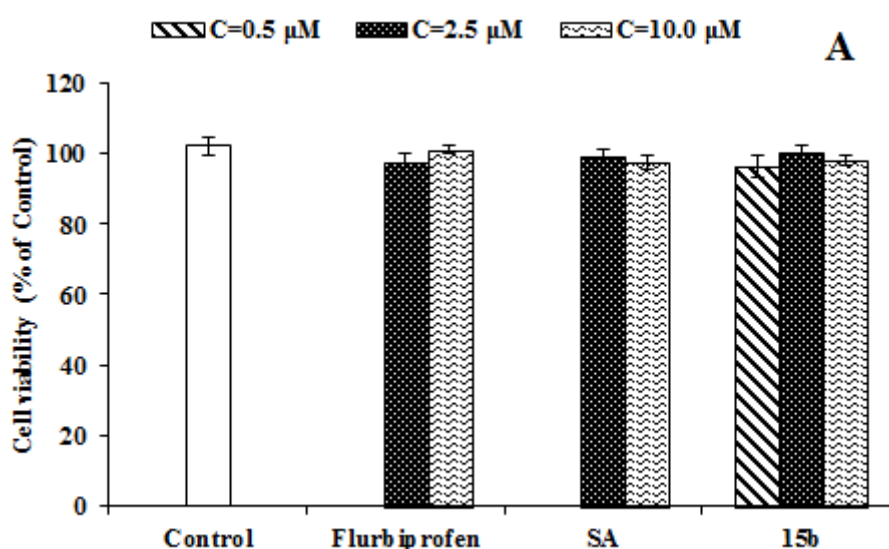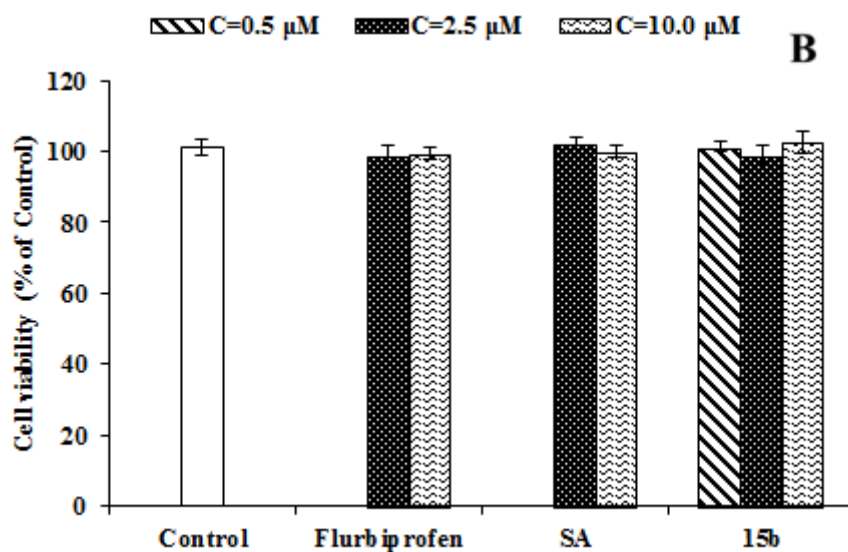
Figure 5. Effects of **SA**, **15b** and flurbiprofen without LPS (**A**) or with LPS (**B**) on the cell viability of microglia BV-2 cells. BV-2 cells were pre-incubated with indicated concentrations of compounds for 30 min followed by 1.0 μg/mL LPS treatment for 24 h. Cell viability was determined by MTT assay. The data are expressed as the mean ± SD from three independent experiments.
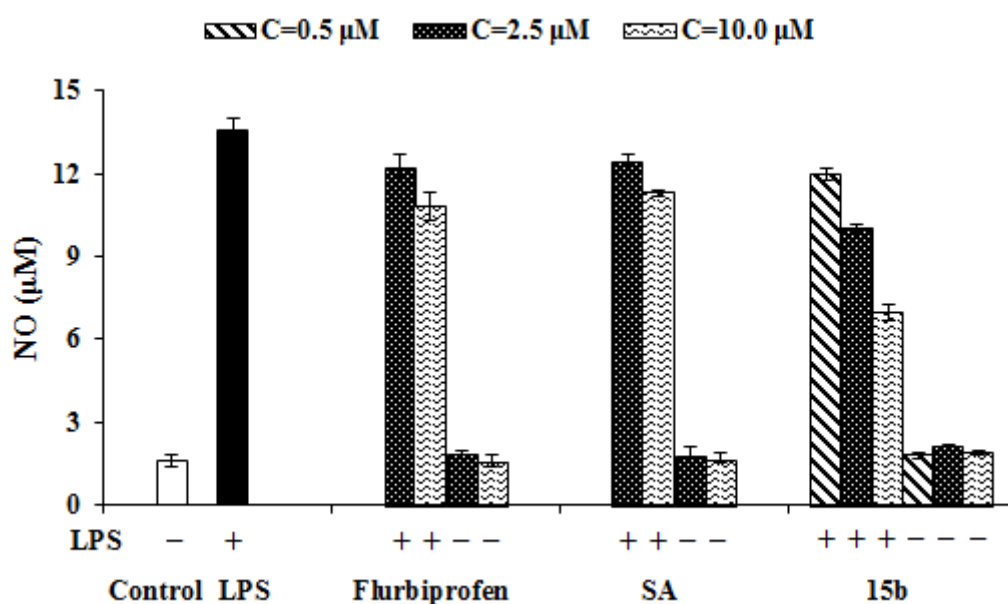
Figure 6. Effects of **SA**, **15b** and flurbiprofen on NO release in BV-2 cells and LPS-stimulated BV-2 cells. The data are expressed as the mean ± SD from three independent experiments.
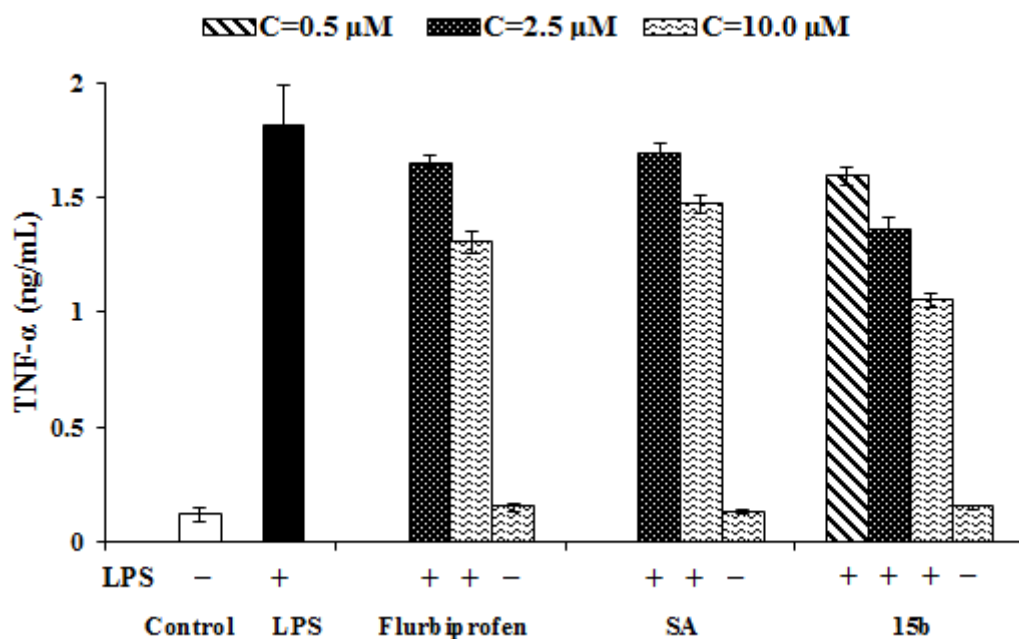
Figure 7. Effects of **SA**, **15b** and flurbiprofen on TNF-α release in LPS-stimulated BV-2 cells. The data are expressed as the mean ± SD from three independent experiments.

3. Conclusion

In summary, a series of salicylamide derivatives were designed, synthesized and evaluated as multifunctional agents for the treatment of AD. *In vitro* assays demonstrated that some compounds possessed moderate AChE inhibitory activity and displayed high selectivity for AChE over BuChE. Most compounds showed good inhibitory activities of self- and Cu^{2+}-induced $A\beta_{1-42}$ aggregation, and significant antioxidant activities. Among them, compound **15b** exhibited a useful inhibitory activity toward RatAChE and EeAChE with IC_{50} value of 10.4 μM and 15.2 μM, respectively. The kinetic analysis suggested that **15b** showed mixed-type inhibition, and could bind to both CAS and PAS of AChE, which was consistent with the molecular modeling study. In addition, **15b** displayed good self- and Cu^{2+}-induced $A\beta_{1-42}$ aggregation inhibitory potency (42.5% and 31.4% at 25 μM, respectively), and moderate disaggregation ability to self- and Cu^{2+}-induced $A\beta_{1-42}$ aggregation fibrils (23.4% and 27.0% at 25 μM, respectively). **15b** also exhibited significant antioxidant activity and good biometal chelating ability. **15b** also possessed the prospective property of acting as anti-neuroinflammatory agent. At last, **15b** could cross the BBB and penetrate into brain. Under the effective treatment concentration, **15b** is worthy of being chosen for further *in vivo* assays to study its

potential effect of multi-target collaborative treatment of AD.

4. Experimental section

4.1 Chemistry

Unless otherwise noted, all materials were obtained from commercial suppliers and used without further purification. Melting points (uncorrected) were measured on YRT-3 melting-point apparatus (China). HPLC analysis was carried out on a Shimadzu LC-10Avp plus system with the use of a Kromasil C_{18} column (4.6 mm × 250 mm, 5 μm). The ^{1}H NMR and ^{13}C NMR spectra were recorded in CDCl$_3$ on a Varian INOVA spectrometer at 25 °C with TMS as the internal standard. Coupling constants are given in Hz. Mass spectra were recorded on Agilent-6210 TOF LC-MS Spectrometer. All the reactions were monitored by thin-layer chromatography (TLC) using silica gel GF$_{254}$ plates from Qingdao Haiyang Chemical Co. Ltd. (China) and the spots were detected under UV light (254 nm). Column chromatography was performed using silica gel (230-400 mesh) purchased from Qingdao Haiyang Chemical Co. Ltd. (China).

4.1.1 Potassium 1,3-dioxoisoindolin-2-ide (2)

Compound 2 was prepared as previously described [30].

4.1.2 General procedure for the synthesis of 3-5

To a mixture of dibromoalkane (32.0 mmol), PEG400 (0.23 mL) in acetone (60 mL), compound 2 (2.96 g, 16.0 mmol) was added in portions under refluxing condition. The resulting mixture was heated for 5-8 h. After the reaction was finished, the solvent was evaporated under reduced pressure. Then water (50 mL) was added to the residue and the mixture was extracted with dichloromethane (50 mL×3). The combined organic phases were washed with brine, dried over sodium sulfate, filtered and concentrated under reduced pressure. The obtained residue was recrystallized from ethanol to afford compound 3-5.

4.1.2.1 2-(3-Bromopropyl)isoindoline-1,3-dione (3)

Compound 3 was synthesized from 2 and 1,3-dibromopropane according to the general procedure; white solid; yield: 75.3%; mp 70-71 °C (Lit. [49] 72-75 °C).

4.1.2.2 2-(4-Bromobutyl)isoindoline-1,3-dione (4)

Compound 4 was synthesized from 2 and 1,4-dibromobutane according to the general procedure;

white solid; yield: 75.9%; mp 79-80 ℃ (Lit. [30] 79-81 ℃).

4.1.2.3 2-(6-Bromohexyl)isoindoline-1,3-dione (*5*)

Compound **5** was synthesized from **2** and 1,6-dibromohexane according to the general procedure; white solid; yield: 70.0%; mp 57-58 ℃ (Lit. [30] 57-58 ℃).

4.1.3 General procedure for the synthesis of *7-9*

To a suspension of the corresponding secondary amine (3.22mmol) and anhydrous K_2CO_3 (765mg, 5.48mmol) in CH_3CN (20 mL) was added the intermediates **3-5** (0.60 mmol). The mixture was refluxed for 6-8 h. The solvent was removed under reduced pressure. The residue was diluted with water (30mL) and the mixture was extracted with dichloromethane (30mL×3). The combined organic phases were washed with brine, dried over sodium sulfate, filtered and concentrated under reduced pressure. The residue was purified on a silica gel chromatography in petroleum ether/acetone (20/1, v/v) to afford compound **7-9**.

4.1.3.1 2-(3-(Benzyl(methyl)amino)propyl)isoindoline-1,3-dione (*7a*)

Compound **7a** was synthesized from **3** and **6a** according to the general procedure; colorless oil; yield: 80.0%; ^{1}H NMR (400 MHz, CDCl$_3$) δ 7.84-7.82 (m, 2H), 7.72-7.69 (m, 2H), 7.29-7.23 (m, 5H), 3.76 (t, *J* = 7.2 Hz, 2H), 3.48 (s, 2H), 2.45 (t, *J* = 7.2 Hz, 2H), 2.17 (s, 3H), 1.92-1.88 (m, 2H).

4.1.3.2 2-(4-(Ethyl(2-methoxybenzyl)amino)propyl)isoindoline-1,3-dione (*7b*)

Compound **7b** was synthesized from **3** and **6d** according to the general procedure; colorless oil; yield: 85.3%; ^{1}H NMR (400 MHz, CDCl$_3$) δ 7.84-7.82 (m, 2H), 7.72-7.69 (m, 2H), 7.43 (d, *J* = 7.2 Hz, 1H), 7.20 (t, *J* = 7.2 Hz, 1H), 6.90 (t, *J* = 7.2 Hz, 1H), 6.83 (d, *J* = 7.2 Hz, 1H), 3.82 (s, 3H), 3.72 (t, *J* = 6.8 Hz, 2H), 3.70 (s, 2H), 2.65-2.57 (m, 4H), 1.96-1.91 (m, 2H), 1.11 (t, *J* = 7.2 Hz, 3H).

4.1.3.3 2-(4-(Benzyl(methyl)amino)butyl)isoindoline-1,3-dione (*8a*)

Compound **8a** was synthesized from **4** and **6a** according to the general procedure; colorless oil; yield: 71.5%; ^{1}H NMR (400 MHz, CDCl$_3$) δ 7.85-7.83 (m, 2H), 7.71-7.70 (m, 2H), 7.29-7.22 (m, 5H), 3.69 (t, *J* = 7.2 Hz, 2H), 3.51 (s, 2H), 2.43 (t, *J* = 6.8 Hz, 2H), 2.19 (s, 3H), 1.72-1.68 (m, 2H), 1.60-1.56 (m, 2H).

4.1.3.4 2-(4-(Benzyl(ethyl)amino)butyl)isoindoline-1,3-dione (*8b*)

Compound **8b** was synthesized from **4** and **6b** according to the general procedure; colorless oil; yield: 81.8%; ^{1}H NMR (400 MHz, CDCl$_3$) δ 7.85-7.83 (m, 2H), 7.73-7.71 (m, 2H), 7.33 (d, *J* = 6.8 Hz, 2H), 7.29 (t, *J* = 6.8 Hz, 2H), 7.22 (t, *J* = 6.8 Hz, 1H), 3.67 (t, *J* = 7.2 Hz, 2H), 3.58 (s, 2H),

2.57-2.46 (m, 4H), 1.71-1.66 (m, 2H), 1.56-1.52 (m, 2H), 1.02 (t, J = 7.2 Hz, 3H).

*4.1.3.5 2-(4-((2-Methoxybenzyl)(methyl)amino)butyl)isoindoline-1,3-dione (**8c**)*

Compound **8c** was synthesized from **4** and **6c** according to the general procedure; colorless oil; yield: 71.8%; ^{1}H NMR (400 MHz, CDCl₃) δ 7.85-7.83 (m, 2H), 7.73-7.71 (m, 2H), 7.30 (d, J = 7.2 Hz, 1H), 7.21 (t, J = 7.2 Hz, 1H), 6.91 (t, J = 7.2 Hz, 1H), 6.85 (d, J = 7.2 Hz, 1H), 3.81 (s, 3H), 3.71 (t, J = 6.8 Hz, 2H), 3.49 (s, 2H), 2.44 (t, J = 7.2 Hz, 2H), 2.20 (s, 3H), 1.74-1.69 (m, 2H), 1.62-1.59 (m, 2H).

*4.1.3.6 2-(4-(Ethyl(2-methoxybenzyl)amino)butyl)isoindoline-1,3-dione (**8d**)*

Compound **8d** was synthesized from **4** and **6d** according to the general procedure; colorless oil; yield: 87.2%; ^{1}H NMR (400 MHz, CDCl₃) δ 7.84-7.81 (m, 2H), 7.72-7.69 (m, 2H), 7.39 (d, J = 7.2 Hz, 1H), 7.19 (t, J = 7.2 Hz, 1H), 6.91 (t, J = 7.2 Hz, 1H), 6.83 (d, J = 7.2 Hz, 1H), 3.81 (s, 3H), 3.68 (t, J = 6.8 Hz, 2H), 3.57 (s, 2H), 2.53-2.47 (m, 4H), 1.73-1.66 (m, 2H), 1.56-1.51 (m, 2H), 1.04 (t, J = 7.2 Hz, 3H).

*4.1.3.7 2-(4-((2-(Dimethylamino)benzyl)(ethyl)amino)butyl)isoindoline-1,3-dione(**8e**)*

Compound **8e** was synthesized from **4** and **6e** according to the general procedure; colorless oil; yield: 84.0%; ^{1}H NMR (400 MHz, CDCl₃) *δ* 7.84-7.82 (m, 2H), 7.71-7.69 (m, 2H), 7.56 (d, J = 7.2 Hz, 1H), 7.17 (t, J = 7.2 Hz, 1H), 7.06-7.00 (m, 2H), 3.67 (t, J = 7.2 Hz, 2H), 3.60 (s, 2H), 2.66 (s, 6H), 2.50-2.45 (m, 4H), 1.70-1.67 (m, 2H), 1.53-1.49 (m, 2H), 1.02 (t, J = 6.8 Hz, 3H).

*4.1.3.8 2-(4-((4-(Dimethylamino)benzyl)(ethyl)amino)butyl)isoindoline-1,3-dione(**8f**)*

Compound **8f** was synthesized from **4** and **6f** according to the general procedure; colorless oil; yield: 77.1%; ^{1}H NMR (400 MHz, CDCl₃) *δ* 7.84-7.82 (m, 2H), 7.71-7.69 (m, 2H), 7.18 (d, J = 8.8 Hz, 2H), 6.68 (d, J = 8.8 Hz, 2H), 3.68 (t, J = 7.2 Hz, 2H), 3.52 (s, 2H), 2.92 (s, 6H), 2.53-2.46 (m, 4H), 1.70-1.66 (m, 2H), 1.57-1.53 (m, 2H), 1.05 (t, J = 7.2 Hz, 3H).

*4.1.3.9 2-(4-(2,3-Dihydrobenzo[f][1,4]oxazepin-4(5H)-yl)butyl)isoindoline-1,3-dione (**8g**)*

Compound **8g** was synthesized from **4** and **6g** according to the general procedure; colorless oil; yield: 81.3%; ^{1}H NMR (400 MHz, CDCl₃) *δ* 7.85-7.82 (m, 2H), 7.73-7.70 (m, 2H), 7.19-7.11 (m, 2H), 7.00-6.95 (m, 2H), 4.04 (t, J = 4.4 Hz, 2H), 3.81 (s, 1H), 3.71 (t, J = 7.2 Hz, 2H), 3.07 (t, J = 4.4 Hz, 2H), 2.50 (t, J = 7.2 Hz, 2H), 1.73-1.67 (m, 2H), 1.60-1.54 (m, 2H).

*4.1.3.10 2-(4-((2-Methoxybenzyl)(prop-2-yn-1-yl)amino)butyl)isoindoline-1,3-dione (**8h**)*

Compound **8h** was synthesized from **4** and **6h** according to the general procedure; colorless oil;

yield: 81.2%; ^{1}H NMR (400 MHz, CDCl$_3$) δ 7.85-7.83 (m, 2H), 7.72-7.70 (m, 2H), 7.35 (d, J = 7.2 Hz, 1H), 7.22 (t, J = 7.2 Hz, 1H), 6.91 (t, J = 7.2 Hz, 1H), 6.85 (d, J = 7.2 Hz, 1H), 3.82 (s, 3H), 3.71 (t, J = 7.2 Hz, 2H), 3.65 (s, 2H), 3.36 (s, 2H), 2.62 (t, J = 7.2 Hz, 2H), 2.23 (s, 1H), 1.78-1.71 (m, 2H), 1.63-1.57 (m, 2H).

*4.1.3.11 2-(6-(Benzyl(methyl)amino)hexyl)isoindoline-1,3-dione (**9a**)*

Compound **9a** was synthesized from **5** and **6a** according to the general procedure; colorless oil; yield: 67.5%; ^{1}H NMR (400 MHz, CDCl$_3$) δ 7.85-7.82 (m, 2H), 7.73-7.70 (m, 2H), 7.29-7.23 (m, 5H), 3.67 (t, J = 7.2 Hz, 2H), 3.48 (s, 2H), 2.36 (q, J = 7.2 Hz, 2H), 2.18 (s, 3H), 1.69-1.66 (m, 2H), 1.55-1.49 (m, 2H), 1.38-1.31 (m, 4H).

*4.1.3.12 2-(6-(Ethyl(2-methoxybenzyl)amino)hexyl)isoindoline-1,3-dione (**9b**)*

Compound **9b** was synthesized from **5** and **6d** according to the general procedure; colorless oil; yield: 67.5%; ^{1}H NMR (400 MHz, CDCl$_3$) δ 7.85-7.83 (m, 2H), 7.72-7.70 (m, 2H), 7.40 (d, J = 8.0 Hz, 1H), 7.20 (t, J = 8.0 Hz, 1H), 6.92 (t, J = 8.0 Hz, 1H), 6.84 (d, J = 8.0 Hz, 1H), 3.81 (s, 3H), 3.66 (t, J = 7.2 Hz, 2H), 3.58 (s, 2H), 2.52 (q, J = 6.8 Hz, 2H), 2.44 (t, J = 6.4 Hz, 2H), 1.68-1.65 (m, 2H), 1.50-1.47 (m, 2H), 1.33-1.31 (m, 4H), 1.04 (t, J = 6.8 Hz, 3H)

*4.1.4 General procedure for the synthesis of **10-12***

To a solution of *N*-aminoalkylphthalimide derivatives **7-9** (4mmol) in ethanol (50ml) was added hydrazine hydrate (1.23ml, 20 mmol). The mixture was refluxed for 6 h. Then the solvent was removed under reduced pressure. The residue was diluted with 5% aqueous sodium hydroxide solution (20mL) and the mixture was stirred for 0.5 h. Then the water (30mL) was added and the mixture was extracted with dichloromethane (30mL×3). The combined organic phases were washed with brine, dried over sodium sulfate, filtered and concentrated under reduced pressure to give compounds **10-12** as colorless oil, which were used without further purification.

*4.1.5 General procedure for the synthesis of (N-aminoalkyl) salicylamide derivatives **13-15***

The mixture of salicylic acid (50.0 mg, 0.362 mmol), the corresponding (*N*-aminoalkyl) salicylamide derivatives **10-12** (0.434 mmol) and EDCI (104 mg, 0.543 mmol) in THF (2 mL) was stirred at room temperature overnight. The solvent was removed under reduced pressure and the residue was diluted with dichloromethane (5mL). The organic phase was washed with saturated solution of NaHCO$_3$ and brine, dried over sodium sulfate, filtered and concentrated under reduced pressure to give the corresponding crude product, which was purified on a silica gel chromatography

using mixtures of CH_2Cl_2/acetone as eluent, obtaining the corresponding (*N*-aminoalkyl) salicylamide derivatives **13-15**.

*4.1.5.1 N-(3-(Benzyl(methyl)amino)propyl)-2-hydroxybenzamide (**13a**)*

Compound **13a** was synthesized from salicylic acid and **10a** according to the general procedure; purification: CH_2Cl_2/acetone (1/4, v/v); colorless oil; yield: 63.0%; MS (ESI) m/z 299.1 [M+H]$^+$; ^{1}H NMR (400 MHz, CDCl$_3$) δ 12.73 (brs, 1H), 8.83 (brs, 1H), 7.35-7.26 (m, 6H), 7.13-7.11 (m, 1H), 6.95 (d, *J* = 8.4 Hz, 1H), 6.63 (t, *J* = 7.6 Hz, 1H), 3.61-3.57 (m, 4H), 2.70 (t, *J* = 5.2 Hz, 2H), 2.31 (s, 3H), 1.85-1.80 (m, 2H); ^{13}C NMR (100 MHz, CDCl$_3$) δ 169.8, 161.5, 137.2, 133.6, 129.6, 128.5, 127.6, 125.8, 118.4, 118.1, 114.4, 63.1, 57.2, 41.2, 40.1, 24.5.

*4.1.5.2 N-(3-(Ethyl(2-methoxybenzyl)amino)propyl)-2-hydroxybenzamide (**13b**)*

Compound **13b** was synthesized from salicylic acid and **10b** according to the general procedure; purification: CH_2Cl_2/acetone (1/1, v/v); colorless oil; yield: 64.2%; MS (ESI) m/z 343.2 [M+H]$^+$; ^{1}H NMR (400 MHz, CDCl$_3$) δ 12.88 (brs, 1H), 9.30 (brs, 1H), 7.34-7.26 (m, 4H), 6.95-6.90 (m, 2H), 6.80 (d, *J* = 8.0 Hz, 1H), 6.49 (brs, 1H), 3.70 (s, 2H), 3.61 (s, 3H), 3.56 (t, *J* = 5.2 Hz, 2H), 2.80-2.70 (m, 4H), 2.00-1.85 (m, 2H), 1.08 (brs, 3H); ^{13}C NMR (100 MHz, CDCl$_3$) δ 169.8, 161.4, 157.8, 133.3, 131.9, 129.3, 126.2, 124.4, 120.2, 118.2, 117.9, 114.3, 110.5, 54.8, 53.1, 52.7, 46.7, 40.6, 23.8, 9.8.

*4.1.5.3 N-(4-(Benzyl(methyl)amino)butyl)-2-hydroxybenzamide (**14a**)*

Compound **14a** was synthesized from salicylic acid and **11a** according to the general procedure; purification: CH_2Cl_2/acetone (3/1, v/v); colorless oil; yield: 46.2%; MS (ESI) m/z 313.2 [M+H]$^+$; ^{1}H NMR (400 MHz, CDCl$_3$) δ 12.52 (brs, 1H), 7.85 (brs, 1H), 7.41-7.28 (m, 7H), 6.96 (d, *J* = 8.4 Hz, 1H), 6.71 (t, *J* = 7.6 Hz, 1H), 3.65 (s, 2H), 3.50-3.44 (m, 2H), 2.58-2.52 (m, 2H), 2.27 (s, 3H), 1.78-1.70 (m, 4H); ^{13}C NMR (100 MHz, CDCl$_3$) δ 170.1, 161.3, 136.6, 133.7, 129.4, 128.4, 127.6, 125.9, 118.4, 118.1, 114.5, 61,5, 56.3, 41.9, 39.1, 26.6, 24.3.

*4.1.5.4 N-(4-(Benzyl(ethyl)amino)butyl)-2-hydroxybenzamide (**14b**)*

Compound **14b** was synthesized from salicylic acid and **11b** according to the general procedure; purification: CH_2Cl_2/acetone (3/1, v/v); colorless oil; yield: 56.8%; MS (ESI) m/z 327.3 [M+H]$^+$; ^{1}H NMR (400 MHz, CDCl$_3$) δ 12.47 (brs, 1H), 7.37-7.26 (m, 7H), 7.17 (brs, 1H), 6.96 (d, *J* = 8.0 Hz, 1H), 6.77 (t, *J* = 7.6 Hz, 1H), 3.65 (s, 2H), 3.46-3.40 (m, 2H), 2.62-2.52 (m, 4H), 1.72-1.62 (m, 4H), 1.08 (t, *J* = 7.2 Hz, 3H); ^{13}C NMR (100 MHz, CDCl$_3$) δ 169.9, 161.2, 137.6, 133.8, 129.2, 128.3,

127.3, 125.9, 118.4, 118.1, 114.5, 57.5, 52.1, 47.0, 39.1, 26.9, 24.1, 10.7.

4.1.5.5 2-Hydroxy-N-(4-((2-methoxybenzyl)(methyl)amino)butyl)benzamide (14c)

Compound **14c** was synthesized from salicylic acid and **11c** according to the general procedure; purification: CH_2Cl_2/acetone (2/1, v/v); colorless oil; yield: 43.1%; MS (ESI) m/z 343.0 [M+H]$^+$; ^{1}H NMR (400 MHz, CDCl$_3$) δ 8.59 (brs, 1H), 7.38 (d, J = 7.6 Hz, 1H), 7.34-7.28 (m, 3H), 6.97-6.86 (m, 3H), 6.56 (t, J = 7.2 Hz, 1H), 3.76 (s, 3H), 3.71 (s, 2H), 3.45 (t, J = 5.6 Hz, 2H), 2.62 (t, J = 6.0 Hz, 2H), 2.26 (s, 3H), 1.84-1.78 (m, 4H); ^{13}C NMR (100 MHz, CDCl$_3$) δ 170.0, 161.2, 157.8, 133.5, 132.0, 129.5, 126.3, 123.4, 120.3, 118.2, 117.8, 114.6, 110.4, 56.4, 55.2, 55.0, 42.0, 38.7, 26.2, 23.9.

4.1.5.6 N-(4-(Ethyl(2-methoxybenzyl)amino)butyl)-2-hydroxybenzamide (14d)

Compound **14d** was synthesized from salicylic acid and **11d** according to the general procedure; purification: CH_2Cl_2/acetone (1/1, v/v); colorless oil; yield: 46.5%; MS (ESI) m/z 357.1 [M+H]$^+$; ^{1}H NMR (400 MHz, CDCl$_3$) δ 8.22 (brs, 1H), 7.57 (brs, 1H), 7.44 (d, J = 7.2 Hz, 1H), 7.32 (t, J = 8.0 Hz, 2H), 6.98-6.87 (m, 3H), 6.69 (t, J = 7.2 Hz, 1H), 3.88 (s, 2H), 3.80 (s, 3H), 3.46 (t, J = 6.0 Hz, 2H), 2.80-2.72 (m, 4H), 1.86-1.73 (m, 4H), 1.16 (t, J = 6.8 Hz, 3H); ^{13}C NMR (100 MHz, CDCl$_3$) δ 170.1, 161.2, 157.8, 133.6, 131.8, 129.8, 126.6, 122.4, 120.5, 118.3, 117.8, 114.5, 110.5, 55.2, 51.9, 51.0, 47.3, 38.5, 26.4, 23.2, 9.6.

4.1.5.7 N-(4-((2-(Dimethylamino)benzyl)(ethyl)amino)butyl)-2-hydroxybenzamide (14e)

Compound **14e** was synthesized from salicylic acid and **11e** according to the general procedure; purification: CH_2Cl_2/acetone (3/2, v/v); colorless oil; yield: 73.7%; MS (ESI) m/z 370.2 [M+H]$^+$; ^{1}H NMR (400 MHz, CDCl$_3$) δ 7.93 (brs, 1H), 7.73 (d, J = 6.4 Hz, 1H), 7.68 (d, J = 7.2 Hz, 1H), 7.34-7.26 (m, 2H), 7.15 (d, J = 8.0 Hz, 1H), 7.09 (t, J = 7.2 Hz, 1H), 6.92 (d, J = 7.6 Hz, 1H), 6.79 (t, J = 7.6 Hz, 1H), 3.98 (s, 2H), 3.45 (t, J = 6.0 Hz, 2H), 2.80-2.75 (m, 4H), 2.64 (s, 6H), 1.80-1.77 (m, 2H), 1.69-1.66 (m, 2H), 1.15 (t, J = 7.2 Hz, 3H); ^{13}C NMR (100 MHz, CDCl$_3$) δ 170.0, 161.0, 153.1, 133.5, 130.8, 129.0, 128.7, 126.8, 124.0, 119.7, 118.4, 117.7, 114.6, 52.1, 51.8, 47.1, 45.1, 38.3, 26.3, 22.7, 9.6.

4.1.5.8 N-(4-((4-(Dimethylamino)benzyl)(ethyl)amino)butyl)-2-hydroxybenzamide (14f)

Compound **14f** was synthesized from salicylic acid and **11f** according to the general procedure; purification: CH_2Cl_2/acetone (3/2, v/v); pale yellow oil; yield: 41.4%; MS (ESI) m/z 370.1 [M+H]$^+$; ^{1}H NMR (400 MHz, CDCl$_3$) δ 10.20 (brs, 1H), 8.20 (brs, 1H), 7.72 (d, J = 8.0 Hz, 1H), 7.34 (t, J = 8.0 Hz, 1H), 7.26 (d, J = 8.4 Hz, 2H), 6.93 (d, J = 8.0 Hz, 1H), 6.80 (t, J = 8.0 Hz, 1H), 6.66 (d, J =

24

8.4 Hz, 2H), 3.79 (s, 2H), 3.46 (t, J = 6.0 Hz, 2H), 2.93 (s, 6H), 2.81-2.70 (m, 4H), 1.84-1.77 (m, 2H), 1.73-1.67 (m, 2H), 1.21 (t, J = 7.2 Hz, 3H); ^{13}C NMR (100 MHz, CDCl₃) δ 170.1, 161.2, 150.4, 133.6, 131.0, 126.7, 119.9, 118.5, 117.9, 114.6, 112.2, 56.3, 51.2, 46.3, 40.3, 40.2, 38.4, 26.4, 22.7, 9.6.

*4.1.5.9 N-(4-(2,3-Dihydrobenzo[f][1,4]oxazepin-4(5H)-yl)butyl)-2-hydroxybenzamide (**14g**)*

Compound **14g** was synthesized from salicylic acid and **11g** according to the general procedure; purification: CH₂Cl₂/acetone (3/1, v/v); colorless oil; yield:50.4%; MS (ESI) m/z 341.2 [M+H]⁺; ^{1}H NMR (400 MHz, CDCl₃) δ 12.44 (brs, 1H), 7.37 (t, J = 8.0 Hz, 1H), 7.30 (d, J = 8.0 Hz, 1H), 7.20 (t, J = 8.0 Hz, 1H), 7.13 (d, J = 6.4 Hz, 1H), 7.03-6.98 (m, 3H), 6.78 (t, J = 8.0 Hz, 1H), 4.07 (t, J = 4.4 Hz, 2H), 3.88 (s, 2H), 3.50-3.42 (m, 2H), 3.12 (t, J = 4.4 Hz, 2H), 2.53 (t, J = 6.8 Hz, 2H), 1.76-1.62 (m, 4H); ^{13}C NMR (100 MHz, CDCl₃) δ 169.9, 161.2, 159.6, 133.8, 130.7, 130.6, 128.7, 125.6, 123.4, 120.7, 118.5, 118.2, 114.4, 69.2, 57.9, 57.8, 52.7, 39.3, 26.9, 24.7.

*4.1.5.10 2-Hydroxy-N-(4-((2-methoxybenzyl)(prop-2-yn-1-yl)amino)butyl)benzamid (**14h**)*

Compound **14h** was synthesized from salicylic acid and **11h** according to the general procedure; purification: CH₂Cl₂/acetone (25/1, v/v); colorless oil; yield:33.1%; MS (ESI) m/z 367.2 [M+H]⁺; ^{1}H NMR (400 MHz, CDCl₃) δ 12.61 (brs, 1H), 7.82 (brs, 1H), 7.35 (d, J = 7.6 Hz, 1H), 7.31-7.25 (m, 2H), 7.09 (d, J = 8.0 Hz, 1H), 6.97-6.90 (m, 2H), 6.85 (d, J = 8.0 Hz, 1H), 6.49 (t, J = 7.6 Hz, 1H), 3.75 (s, 3H), 3.69 (s, 2H), 3.44 (q, J = 5.6 Hz, 2H), 3.26 (d, J = 2.4 Hz, 2H), 2.67 (t, J = 6.0 Hz, 1H), 2.26 (t, J = 2.4 Hz, 1H), 1.83-1.69 (m, 4H); ^{13}C NMR (100 MHz, CDCl₃) δ 169.9, 161.4, 157.8, 133.6, 131.4, 129.0, 125.6, 125.5, 120.3, 118.2, 118.2, 114.5, 110.4, 78.1, 73.8, 55.0, 52.9, 51.1, 42.4, 39.2, 26.5, 24.8.

*4.1.5.11 N-(6-(Benzyl(methyl)amino)hexyl)-2-hydroxybenzamide (**15a**)*

Compound **15a** was synthesized from salicylic acid and **12a** according to the general procedure; purification: CH₂Cl₂/acetone (2/1, v/v); colorless oil; yield:65.0%; MS (ESI) m/z 341.3 [M+H]⁺; ^{1}H NMR (400 MHz, CDCl₃) δ 7.43 (d, J = 7.6 Hz, 1H), 7.39-7.26 (m, 6H), 6.97 (d, J = 8.4 Hz, 1H), 6.84 (t, J = 7.6 Hz, 1H), 6.59 (brs, 1H), 3.61 (s, 2H), 3.43 (q, J = 6.4 Hz, 2H), 2.46 (t, J = 7.2 Hz, 2H), 2.28 (s, 3H), 1.64-1.59 (m, 4H), 1.42-1.34 (m, 4H); ^{13}C NMR (100 MHz, CDCl₃) δ 169.7, 160.9, 137.4, 133.8, 129.3, 128.2, 127.2, 126.0, 118.6, 118.2, 114.8, 61.8, 56.8, 41.6, 39.4, 29.2, 26.7, 26.5.

*4.1.5.12 N-(6-(Ethyl(2-methoxybenzyl)amino)hexyl)-2-hydroxybenzamide (**15b**)*

Compound **15b** was synthesized from salicylic acid and **12b** according to the general procedure;

purification: CH$_2$Cl$_2$/acetone (2/1, v/v); colorless oil; yield:43.0%; MS (ESI) m/z 385.2 [M+H]$^+$; ^{1}H NMR (400 MHz, CDCl$_3$) δ 7.46 (d, J = 7.6 Hz, 2H), 7.37 (t, J = 7.6 Hz, 1H), 7.26-7.23 (m, 1H), 6.98-6.91 (m, 2H), 6.88-6.82 (m, 2H), 6.69 (brs, 1H), 3.82 (s, 3H), 3.74 (s, 2H), 3.46-3.41 (m, 2H), 2.67-2.63 (m, 2H), 2.56 (t, J = 7.2 Hz, 2H), 1.64-1.59 (m, 4H), 1.42-1.32 (m, 4H), 1.13 (t, J = 6.8 Hz, 3H); ^{13}C NMR (100 MHz, CDCl$_3$) δ 169.7, 161.1, 157.7, 133.7, 130.9, 128.6, 126.2, 125.0, 120.4, 118.5, 118.2, 114.9, 110.3, 55.3, 52.7, 50.9, 47.3, 39.4, 29.1, 26.7, 26.5, 25.8, 10.8.

4.2 Biological evaluation

4.2.1 Inhibition experiments of AChE and BuChE

To determine the *in vitro* cholinesterase activities of the compounds, the spectrophotometric method of Ellman was performed [32, 33], using AChE from 5% rat cortex homogenate, purified AChE from *Electrophorus electricus* (Sigma-Aldrich Co.) and BuChE from rat serum. The brain homogenate was preincubated with tetraisopropyl pyrophosphoramide (*iso*-OMPA, selective inhibitor of BuChE, 4.0 mmol/L, Sigma-Aldrich Co.) for 5 min before use. For rat AChE or BuChE inhibition assays, the reaction mixture (100 μL) consisted of acetylthiocholine iodide (1 mmol/L, 30 μL) (J&K Scientific) or butyrylthiocholine iodide (1 mmol/L, 30 μL) (TCI Shanghai Development), phosphate-buffered solution (0.1 mmol/L, pH = 7.40, 40 μL), 5% homogenate or 25% serum (10 μL) and different concentrations of test compounds (20 μL). The mixture was incubated at 37 °C for 15 min, followed by the addition of 5,5'-dithiobis-2-nitrobenzoic acid (DTNB, 0.2%, 30 μL) (J&K Scientific) to produce the yellow anion of 5-thio-2-nitrobenzoic acid. Changes in absorbance were detected at 405 nm in a Varioskan Flash Multimode Reader (Thermo Scientific). For *Ee*AChE inhibition assay, *Ee*AChE (0.05 U/mL, final concentration) was used and the assay was carried out in a phosphate buffer (0.01 mmol/L, pH = 8.00). Changes in absorbance were detected at 412 nm. The other procedure was the same as above. The inhibitory activities of compounds toward AChE or BuChE would reduce the color generation and IC$_{50}$ values were calculated as the concentration of compound that produces 50% AChE or BuChE activity inhibition. Donepezil was applied as the positive drug. All samples were assayed in triplicate.

4.2.2 Kinetic study for the inhibition of AChE

Kinetic characterization of AChE inhibition was carried out based on a reported method using purified AChE from *E. Electricus* (*Ee*AChE) [34]. The assay solution (100 μL) consists of 0.1 M

phosphate buffer (pH 8.00), with the addition of 30 μL of 0.2% DTNB, 10 μL of 0.5 U/mL *Ee*AChE, and 20 μL of substrate (ATCh). Three different concentrations of inhibitors were added to the assay solution and pre-incubated with the *Ee*AChE for 15 min at 37°C, followed by the addition of substrate in different concentrations. Kinetic characterization of the hydrolysis of ATCh catalyzed by *Ee*AChE was done spectra-metrically at 274 nm. The parallel control experiments were performed without inhibitor. The plots were assessed by a weighted least square analysis that assumed the variance of v to be a constant percentage of v for the entire data set. Slopes of reciprocal plots were then plotted against the concentration of **15b** in a weighted analysis, and K_i was determined as the intercept on the negative x-axis.

4.2.3 Molecular modeling study

The crystal structure of AChE complexed with donepezil (PDB code: *1EVE*) was obtained from the Protein Data Bank after removing the original inhibitors and water molecules [35]. The 3D Structure of **15b** was built and performed geometry optimization by molecular mechanics. After addition of Gasteiger charges, removal of hydrogen atoms, addition of their atomic charges to skeleton atoms, and the assignment of proper atomic types, the further preparation of the inhibitor was accomplished. Autotors was then used to define the rotatable bonds in the ligands. Docking studies were performed using the AUTODOCK 4.2 program. By using Autodock Tools (ADT; version 1.5.6), polar hydrogen atoms were added to amino acid residues, and Gasteiger charges were assigned to all atoms of the enzyme. The resulting enzyme structure was used as an input for the AUTOGRID program. AUTOGRID performed a pre-calculated atomic affinity grid maps for each atom type in the ligand, plus an electrostatics map and a separate desolvation map presented in the substrate molecule. All maps were calculated with 0.375 Å spacing between grid points. The center of the grid box was placed at the center of donepezil with coordinates $x = 2.023$, $y = 63.295$, $z = 67.062$. The dimensions of the active site box were set at $60 \times 60 \times 60$ Å. Flexible ligand docking was performed for the compounds. Each docked system was performed by 100 runs of the AUTODOCK search by the Lamarckian genetic algorithm (LGA). Other than the referred parameters above, the other parameters were accepted as default. A cluster analysis was performed on the docking results using a root mean square (RMS) tolerance of 1.0 and the lowest energy conformation of the highest populated cluster was selected for analysis. Graphic manipulations and visualizations were done by Autodock Tools or Discovery Studio 2.5 software.

4.2.4 Antioxidant activity assay

The antioxidant potency was evaluated by the oxygen radical absorbance capacity-fluorescein (ORAC-FL) assay [36]. Fluorescein (FL) and 6-hydroxy-2,5,7,8-tetramethylchromane-2-carboxylic acid (Trolox) were purchased from TCI (Shanghai) Development. 2,2'-Azobis(amidinopropane) dihydrochloride (AAPH) was purchased from Accela ChemBio Co. Ltd. All the assays were performed with 75 mM phosphate buffer (pH = 7.40), and the final reaction mixture was 200 μL. FL (120 μL, 150 nM final concentration) and antioxidant (20 μL) were added in the wells of a black 96-well plate using Trolox as a standard (1-8 μM, final concentration). The plate was incubated for 15 min at 37 °C and then placed in a Varioskan Flash Multimode Reader (Thermo Scientific). AAPH solution (60 μL, 12 mM final concentration) was added rapidly using an autosampler and the fluorescence recorded every minute for 90 min with excitation at 485 nm and emission at 535 nm. The plate was automatically shaken prior to each reading. A blank (FL + AAPH) using phosphate buffer instead of antioxidant and Trolox calibration were carried out in each assay. The samples were measured at different concentrations (1-10 μM). All the reaction mixture was prepared in duplicate, and at least three independent assays were performed for each sample. Antioxidant curves (fluorescence versus time) were normalized to the curve of the blank in the same assay, and then the area under the fluorescence decay curve (AUC) was calculated. The net AUC of a sample was obtained by subtracting the AUC of the blank. ORAC-FL values were expressed as Trolox equivalents by using the standard curve calculated for each sample, where the ORAC-FL value of Trolox was taken as 1, indicating the antioxidant potency of the tested compounds.

4.2.5 Metal-chelating studies [37, 38]

The chelating studies were performed using a Varioskan Flash Multimode Reader (Thermo Scientific). The UV absorption spectra of tested compound alone or in the presence of $CuCl_2$, $ZnCl_2$, $AlCl_3$, and $FeSO_4$ were recorded with wavelength ranging from 200 to 600 nm after incubating for 30 min in methanol at room temperature. The final volume of reaction mixture was 200 μL, and the final concentrations of tested compound and metals were 37.5 μM. The difference UV-vis spectra due to complex formation were obtained by numerical subtraction of the spectra of the metal alone and the compound alone from the spectra of the mixture.

The stoichiometry of the compound-Cu^{2+} complex was determined by titrating the methanol solution of tested compound with ascending of $CuCl_2$. The final concentration of tested compound

was 37.5 μM, and the final concentration of $CuCl_2$ ranged from 3.75 to 150 μM. The UV spectra were recorded and treated by numerical subtraction of $CuCl_2$ and tested compound at corresponding concentrations, plotted versus the mole fraction of tested compound.

4.2.6 Inhibition of self- and Cu^{2+}-induced $A\beta_{1-42}$ aggregation

In order to investigate the self-induced $A\beta_{1-42}$ aggregation, a Thioflavin T-based fluorometric assay was performed [39-42]. Thioflavin T (ThT) was purchased from TCI (Shanghai) Development. 1,1,1,3,3,3-hexafluoro-2-propanol (HFIP) was purchased from Energy Chemical. β-Amyloid$_{1-42}$ ($A\beta_{1-42}$), supplied as trifluoroacetate salt, was purchased from GL Biochem Ltd. Briefly, $A\beta_{1-42}$ was dissolved in HFIP (1 mg/mL) and incubation for 24 h at room temperature, then the solvent was evaporated. And it was dissolved in dry DMSO to a final stock concentration of 200 μM and kept frozen at -80 °C. Tested compounds were dissolved in DMSO in 2.5 mM for storage and diluted with phosphate buffer solution (pH 7.4) before use. For the self-induced aggregation assay, $A\beta_{1-42}$ (20 μL, 25 μM, final concentration) together with test compounds (20 μL, 25 μM, final concentration) were incubated in 50 mM phosphate buffer solution (pH 7.40) at 37 °C for 24 h. The plate was sealed with a transparent heat-resistant plastic film to minimize evaporation effect. After the incubation, 160 μL of 5 μM ThT in 50 mM glycine-NaOH buffer (pH 8.5) was added. Each assay was run in triplicate. Fluorescence was measured on a Varioskan Flash Multimode Reader (Thermo Scientific) with excitation and emission wavelengths at 446 nm and 490 nm, respectively. The percent inhibition due to the presence of the inhibitor was calculated by the following expression: $(1-IF_i/IF_c) \times 100$, in which IF_i and IF_c are the fluorescence intensities obtained for $A\beta_{1-42}$ in the presence and in the absence of inhibitors after subtracting the background, respectively.

For the Cu^{2+}-induced $A\beta_{1-42}$ aggregation assay, solutions of Cu^{2+} were prepared from standards to concentration of 75 μM using the HEPES buffer (20 mM, pH 6.60, 150 mM NaCl). The $A\beta_{1-42}$ stock solution was diluted with HEPES buffer (20 mM, pH 6.60, 150 mM NaCl). The mixture of $A\beta_{1-42}$ (20 μL, 25 μM, final concentration) and Cu^{2+} (20 μL, 25 μM, final concentration), with or without the tested compound (20 μL, 25 μM, final concentration) was incubated at 37 °C for 24h. Then, 190 μL of 5 μM ThT in 50 mM glycine-NaOH buffer (pH 8.50) was added. Each assay was run in triplicate. The detection method was the same as that of self-induced $A\beta_{1-42}$ aggregation assay.

4.2.7 Effect on the disaggregation of $A\beta_{1-42}$ aggregation fibrils

For the disaggregation of self-induced $A\beta$ fibrils experiment, the $A\beta_{1-42}$ stock solution was

diluted in HEPES buffer (20 mM, pH6.6, 150 mM NaCl). $A\beta_{1-42}$ (20 mL, 50 mM) was incubated at 37 °C for 24 h. Then the tested compound (20 mL, 25 mM, final concentration) was added and incubated at 37 °C for another 24 h. To minimize evaporation effect the wells were sealed by a transparent heat-resistant plastic film. After incubation, 160 mL of 5 mM ThT in 50 mM glycine-NaOH buffer (pH 8.5) was added. The final concentration of DMSO in each well was 12.5%. Each assay was run in triplicate. The detection method was the same as that of self-induced $A\beta_{1-42}$ experiment.

For the disaggregation of copper-induced $A\beta$ fibrils experiment, the $A\beta_{1-42}$ stock solution was diluted in HEPES buffer (20 mM, pH6.6, 150 mM NaCl). The mixture of the $A\beta_{1-42}$ (20 mL, 25 mM, final concentration) with Cu^{2+} (20 mL, 25 mM, final concentration) was incubated 37 °C for 24 h. The tested compound (20 mL, 25 mM, final concentration) was then added and incubated at 37 °C for another 24 h. To minimize evaporation effect the wells were sealed by a transparent heat-resistant plastic film. After incubation, 190 mL of 5 mM ThT in 50 mM glycine-NaOH buffer (pH 8.5) was added. The final concentration of DMSO in each well was 12.5%. Each assay was run in triplicate. The detection method was the same as above.

4.2.8 In vitro blood-brain barrier permeation assay [43]

The *in vitro* blood-brain barrier permeation assay was conducted using the artificial membrane permeation assay of the blood-brain barrier (PAMPA-BBB) as described by Di *et al*. [44] The donor plate (MATRNPS50) and the acceptor plate (PVDF membrane, pore size 0.45 μm, MAIPN4550) were purchased from Millipore. And porcine brain lipid (PBL) was purchased from Avanti Polar Lipids. Filter PDVF membrane units (diameter 25 mm, pore size 0.45 μm) from Pall Corporation were used to filter the samples. Test compounds were dissolved in DMSO at 5 mg/mL and diluted with PBS/EtOH (70:30) to a final concentration of 100 μg/mL. The filter membrane was coated with 4 μL PBL in dodecane (20 μg/mL) and the acceptor wells were filled with 200 μL of PBS/EtOH (70:30). Then 350 μL of the compound solutions (100 μg/mL) were added to the donor wells. The acceptor filter plate was carefully put on the donor plate, and they were left undisturbed for 18 h at 25 °C. After the incubation, the two plates were separated and the concentrations of drug in the donor and acceptor wells were determined using the Varioskan Flash Multimode Reader (Thermo Scientific). Every sample was analyzed at ten wavelengths in four wells and in at least three independent runs. P_e was calculated using the following expression:

$P_e = - \ln [1 - C_A(t)/C_{equilibrium}]/[A \times (1/V_D + 1/V_A) \times t]$

$C_{equilibrium} = [C_D(t) \times V_D + C_A(t) \times V_A]/(V_D + V_A)$

Where P_e is permeability in the unit of cm/s. $C_A(t)$ is the compound concentration in acceptor well at time t, and $C_D(t)$ is the compound concentration in donor well at time t. A is effective filter area and t is the permeation time. V_D is the volume of donor well and V_A is the volume of acceptor well. Results are given as the mean ± SD. In the experiment, 11 quality control drugs of known BBB permeability were included to validate the analysis set. A plot of the experimental data versus literature values gave a strong linear correlation, P_e (exp.) = 0.9163 × P_e (bibl.)−0.2247 (R^2 = 0.9558). From this equation and referring to the limit established by Di *et al.*[40] for BBB permeation, we determined that compounds with P_e values above 3.44×10^{-6} cm/s could cross the BBB.

4.2.9 In vitro anti-neuroinflammatory activity studies [45-46]

To evaluate the anti-neuroinflammatory activity of these hybrid compounds, the *in vitro* cytotoxicity and inhibition of LPS-induced NO and TNF-*α* production were investigated. BV-2 cell-line was obtained from ATCC, and cells were cultured in Dulbecco's modified eagle medium (DMEM) containing 10% fetal bovine serum, 2 mM glutamine, 1 mM pyruvate, penicillin (100 U/mL) and streptomycin (10 μg/mL) at 37 °C in a humidified incubator with 5% CO_2. DMEM was purchased from Gibco and lipopolysaccharide (LPS) was purchased from Sigma. All test samples were prepared in DMSO and diluted to various concentrations before addition to the experimental wells and the final concentration was 0.5, 2.5 and 10.0 μM respectively.

The *in vitro* cytotoxicity assay was carried out by the MTT method. BV-2 cells prepared in DMEM (100 μL) were cultured in 96-well cell culture microplate and incubated at 37 °C for 24 h in a humidified 5% CO_2 atmosphere. MTT (3-(4,5-dimethylthiazol-2-yl)-2,5-diphenyltetrazolium bromide) was dissolved in PBS at 5 mg/mL and filtered to sterilize and remove a small amount of insoluble residue present in some batches of MTT. The test samples at a volume of 10 μL were added to confluent cells in triplicate wells. After the addition of the test samples, the treated wells were incubated for 30 min. And then LPS (10 μL, 1.0 μg/mL) was added, the treated wells were incubated for another 24 h. After the incubation period, 100 μL of MTT solution was added to each well. The wells were incubated for 4 h. The crystals formed were dissolved in 200 μL of DMSO and the absorbance was detected at 490 nm using a spectrophotometer. Results are expressed as percent viability compared to untreated cells.

Inhibition of LPS-induced NO production was measured by using a Griess reaction method. BV-2 cells prepared in DMEM(100 μL) were cultured in 96-well cell culture microplate and incubated at 37 °C for 24 h in a humidified 5% CO_2 atmosphere. $NaNO_2$ was prepared in the mixture of PBS and DMEM at various concentrations (0, 1.5625, 3.125, 6.25, 12.5, 25, 50 and 100 μM) before addition to the experimental wells. The test samples at a volume of 10 μL were added to confluent cells in triplicate wells. After the addition of the test samples, the treated wells were incubated for 30 min. And then LPS (10 μL, 1.0 μg/mL) was added, BV2-cells were stimulated with LPS in the presence of test samples for 24 h. NO released from BV-2 cells was measured by the determination of $NaNO_2$ concentration in culture supernatant. Samples (50 μL) of culture media were incubated with the same volume of Griess reagent (1% sulfanilamide, 0.1% naphthylethylene diamine in 2.5% phosphoric acid solution) at room temperature for 10 min. Absorbance at 540 nm was read using an ELISA plate reader. Standard calibration curves were prepared using sodium nitrite as standard.

Inhibition of LPS-induced TNF-α production was measured by using an enzyme-linked immunosorbent assay (ELISA). BV-2 cells prepared in DMEM (100 μL) were cultured in 96-well cell culture microplate and incubated at 37 °C for 24 h in a humidified 5% CO_2 atmosphere. The test samples at a volume of 10 μL were added to confluent cells in triplicate wells. After the addition of the test samples, the treated wells were incubated for 30 min. And then LPS (10 μL, 1.0 μg/mL) was added, BV2-cells were stimulated with LPS in the presence of test samples for 24 h. And then the TNF-α released from BV-2 cells was measured by the ELISA assay according to the manufacturer's instructions.

Appendix A. Supplementary Material

The supplementary data associated with this article can be found in the online version.

References

[1] M.C. Carreiras, E. Mendes, M.J. Perry, A.P. Francisco, J. Marco-Contelles, The multifactorial nature of Alzheimer's disease for developing potential therapeutics. Curr. Top. Med. Chem. 13 (2013) 1745-1770.

[2] Y.D. Huang, L. Mucke, Alzheimer mechanisms and therapeutic strategies. Cell 148 (2012) 1204-1222.

[3] Alzheimer's Association, Alzheimer's disease facts and figures. Alzheimer's & Dementia 12 (2016) 459-509.

[4] S.Y. Hung, W.M. Fu, Drug candidates in clinical trials for Alzheimer's disease. J. Biomed. Sci. 24 (2017) 47.

[5] S. Kar, S.P. Slowikowski, D. Westaway, H.T. Mount, Interactions between β-amyloid and central cholinergic neurons:implications for Alzheimer's disease. J. Neuropsychiatry Clin. Neurosci. 29 (2004) 427-441.

[6] D.R. Liston, J.A. Nielsen, A. Villalobos, D. Chapin, S.B. Jones, S.T. Hubbard, I.A. Shalaby, A. Ramirez, D. Nason, W.F. White, Pharmacology of selective acetylcholinesterase inhibitors: implications for use in Alzheimer's disease. Eur. J. Pharmacol. 486 (2004) 9-17.

[7] R. Jakob-Roetne, H. Jacobsen, Alzheimer's disease: from pathology to therapeuticapproaches. Angew. Chem. Int. Ed. 48 (2009) 3030-3059.

[8] V.W. Chow, M.P. Mattson, P.C. Wong, M. Gleichmann, An overview of APP processing enzymes and products. NeuroMol. Med. 12 (2010) 1-12.

[9] A.K. Sharma, S.T. Pavlova, J. Kim, D. Finkelstein, N.J. Hawco, N.P. Rath, J. Kim, L.M. Mirica, Bifunctional compounds for controlling metal-mediated aggregation of the Aβ_{42} peptide. J. Am. Chem. Soc. 134 (2012) 6625-6636.

[10] D.A. Butterfield, M.L. Bader Lange, R. Sultana, Involvements of the lipid peroxidation product, HNE, in the pathogenesis and progression of Alzheimer's disease. Biochim. Biophys. Acta 1801 (2010) 924-929.

[11] C. Cheignon, M. Tomas, D. Bonnefont-Rousselot, P. Faller, C. Hureau, F. Collin, Oxidative stress and the amyloid beta peptide in Alzheimer's disease. Redox Biol. 14 (2018) 450-464.
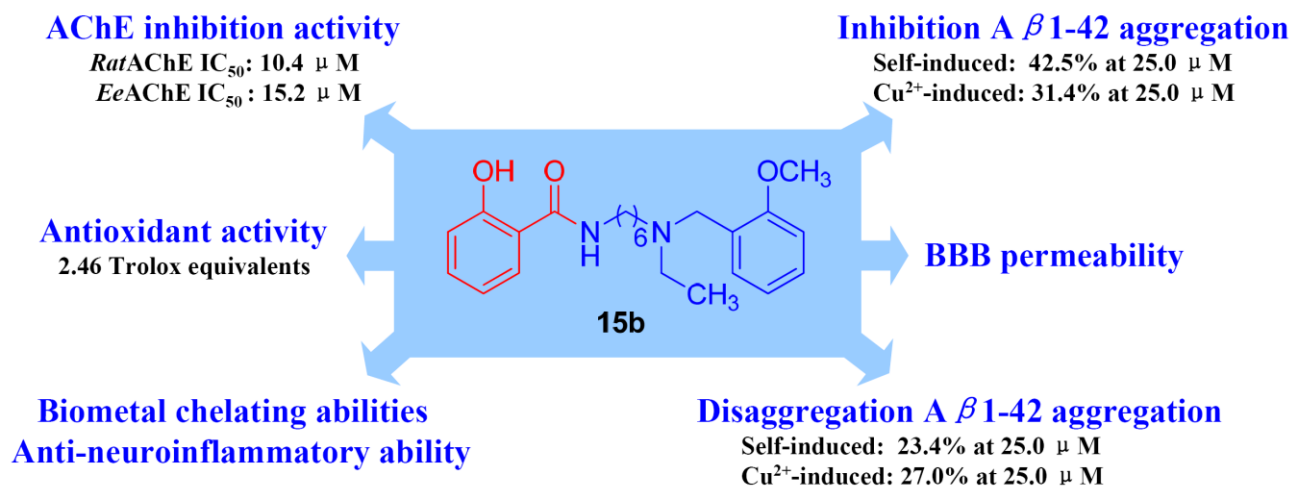
[12] X. Wang, W. Wang, L. Li, G. Perry, H.G. Lee, X. Zhu, Oxidative stress and mitochondrial dysfunction in Alzheimer's disease. Biochim. Biophys. Acta 1842 (2014) 1240-1247.

[13] T. Azarashvili, R. Stricker, G. Reiser, The mitochondriapermeability transition pore complex in the brain with interactingproteins-promising targets for protection in neurodegenerativediseases. Biol. Chem. 391 (2010) 619-629.

[14] G.Y. Sun, Y. He, D.Y. Chuang, J.C. Lee, Z. Gu, A. Simonyi, A.Y. Sun, Integrating cytosolic phospholipase A_2 with oxidative nitrosative signaling pathways in neurons: a novel therapeuticstrategy for AD. Mol. Neurobiol. 46 (2012) 85-95.

[15] P.B. Shelat, M. Chalimoniuk, J.H. Wang, J.B. Strosznajder, J.C. Lee, A.Y. Sun, A. Simonyi, G.Y. Sun, Amyloid beta peptide and NMDA induce ROS from NADPH oxidase and AA release fromcytosolic phospholipase A_2 in cortical neurons. J. Neurochem. 106 (2008) 45-55.

[16] G. Halliday, S.R. Robinson, C. Shepherd, J. Kril, Alzheimer's disease and inflammation:a review of cellular and therapeutic mechanisms. Clin. Exp. Pharmacol. Physiol. 27 (2000) 1-8.

[17] S.C. Vlad, D.R. Miller, N.W. Kowall, D.T.Felson, Protective effects of NSAIDs on the development of Alzheimer disease. Neurol. 70 (2008) 1672-1677.

[18] S. Venneti, C.A. Wiley, J. Kofler, Imaging microglial activation during neuroinflammation and Alzheimer's disease. J. Neuroimmune Pharmacol. 4 (2009) 227-243.

[19] T. Wyss-Coray, Inflammation in Alzheimer disease: driving force, bystander or beneficial response? Nat. Med. 12 (2006) 1005-1015.

[20] D. Giulian, J. Li, X. Li, J. George, P. Rutecki, The impact of microglia-derived cytokines upon gliosis in the CNS. Dev. Neurosci. 16 (1994) 128-136.

[21] E.G. McGeer, P.L. McGeer, Inflammatory processes in Alzheimer's disease. Prog. Neuro-Psychopharmacol. Biol. Psychiatry. 27 (2003) 741-749.

[22] S. Muraoka, T. Miura, Inactivation of cholinesterase induced by non-steroidal anti-inflammatory drugs with horseradish peroxidase: implication for Alzheimer's disease. Life Sci. 84 (2009) 272-277.

[23] X. Lan, R. Liu, L. Sun, T. Zhang, G. Du, Methyl salicylate 2-O-β-D-lactoside, a novel salicylic acid analogue, acts as an anti-inflammatory agent on microglia and astrocytes. J. Neuroinflammation 8 (2011) 98.

[24] M. Coma, L. Sereno, B. Da Rocha-Souto, T. Scotton, J. España, M. Sánchez, M. Rodríguez, J.

Agulló, C. Guardia-Laguarta, M. Garcia-Alloza, Triflusal reduces dense-core plaque load, associated axonal alterations and inflammatory changes, and rescues cognition in a transgenic mouse model of Alzheimer's disease. Neurobiol. Dis. 38 (2010) 482-491.

[25] Q. Liu, X. Qiang, Y. Li, Z. Sang, Y. Li, Z. Tan, Y. Deng, Design, synthesis and evaluation of chromone-2-carboxamido-alkylbenzylamines as multifunctional agents for the treatment of Alzheimer's disease. Bioorg. Med. Chem. 23 (2015) 911-923.

[26] Z. Rankovic, CNS physicochemical property space shaped by a diverse set of molecules with experimentally determined exposure in the mouse brain. Eur. J. Med. Chem. 60 (2017) 5943-5954.

[27] P.D. Leeson, A.M. Davis, Tine-related differences in the physical property profiles of oral drugs. J. Med. Chem. 47 (2004) 6338-6348.

[28] C.A. Lipinski. Lead- and drug-like compounds: the rule-of-five revolution. Drug Discov. Today Technol. 1 (2004) 337-341.

[29] V.A. Levin, Relationship of octanol/water partition coefficient and molecular weight to rat brain capillary permeability. J. Med. Chem. 23 (1980) 682-684.

[30] X. Kong, Z. He, Y. Zhang, L. Mu, C. Liang, B. Chen, X. Jing, A.N. Cammidge, A mesogenic triphenylene-perylene-triphenylene triad. Org. Lett. 13 (2011) 764-767.

[31] F. Al-Omran ,A.A. El-Khair, Heterocyclic synthesis via enaminones: novel synthesis of (1*H*)-pyridin-2-one, pyrazolo[1,5-a]pyrimidine and isoxazole derivatives incorporating a *N*-methylphthalimide and their biological evaluation. J. Heterocycl. Chem. 42 (2005) 307-312.

[32] X. Yang, X. Qiang, Y. Li, L. Luo, R. Xu, Y. Zheng, Z. Cao, Z. Tan, Y. Deng, Pyridoxine-resveratrol hybrids Mannich base derivatives as novel dual inhibitors of AChE and MAO-B with antioxidant and metal-chelating properties for the treatment of Alzheimer's disease. Bioorg. Chem. 71 (2017) 305-314.

[33] Z. Hailin, M. B. H. Youdim, F. Mati, Selective acetylcholinesterase inhibitor activated by acetylcholinesterase releases an active chelator with neurorescuing and anti-amyloid activities. ACS Chem. Neurosci. 1 (2010) 737-746.

[34] C. Lu, Q. Zhou, J. Yan, Z. Du, L. Huang, X. Li, A novel series of tacrine-selegiline hybrids with cholinesterase and monoamine oxidase inhibition activities for the treatment of Alzheimer's disease. Eur. J. Med. Chem. 62 (2013) 745-753.

[35] Y. He, P. F. Yao, S. B. Chen, Z. H. Huang, S. L. Huang,; J. H. Tan, D. Li, L. Q. Gu, Z. S. Huang, Synthesis and evaluation of 7,8-dehydrorutaecarpine derivatives as potential multifunctional agents for the treatment of Alzheimer's disease. Eur. J. Med. Chem. 63C (2013) 299-312.

[36] A. Dávalos, C. Gómez-Cordovés, B. Bartolomé, Extending applicability of the oxygen radical absorbance capacity (ORAC-fluorescein) assay. J. Agric. Food Chem. 52 (2004) 48-54.

[37] Y. Li, X. Qiang, L. Luo, Y. Li, G. Xiao, Z. Tan, Y. Deng, Synthesis and evaluation of 4-hydroxyl aurone derivatives as multifunctional agents for the treatment of Alzheimer's disease. Bioorg. Med. Chem. 24 (2016) 2342-2351.

[38] L. Huang, C. Lu, Y. Sun, F. Mao, Z. Luo, T. Su, H. Jiang, W. Shan, X. Li, Multitarget-directed benzylideneindanone derivatives: anti-β-amyloid (Aβ) aggregation, antioxidant, metal chelation, and monoamine oxidase B (MAO-B) inhibition properties against Alzheimer's disease. J. Med. Chem. 55 (2012) 8483-8492.

[39] N. García-Font, H. Hayour, A. Belfaitah, J. Pedraz, I. Moraleda, I. Iriepa, A. Bouraiou, M. Chioua, J. Marco-Contelles, M. J. Oset-Gasque, Potent anticholinesterasic and neuroprotective pyranotacrines as inhibitors of beta-amyloid aggregation, oxidative stress and tau-phosphorylation for Alzheimer's disease. Eur. J. Med. Chem. 118 (2016) 178-192.

[40] Z. Sang, X. Qiang, Y. Li, W. Yuan, Q. Liu, Y. Shi, W. Ang, Y. Luo, Z. Tan, Y. Deng, Design, synthesis and evaluation of scutellarein-O-alkylamines as multifunctional agents for the treatment of Alzheimer's disease. Eur. J. Med. Chem. 94 (2015) 348-366.

[41] M. Chioua, J. Pérez-Peña, N. García-Font, I. Moraleda, I. Iriepa, E. Soriano, J. Marco-Contelles, M.J. Oset-Gasque, Pyranopyrazolotacrines as nonneurotoxic, Aβ-anti-aggregating and neuroprotective agents for Alzheimer's disease. Future Med. Chem. 7 (2015) 845-855.

[42] M. Bartolini, C. Bertucci,; M.L. Bolognesi, A. Cavalli, C. Melchiorre, V. Andrisano, Insight into the kinetic of amyloid β (1-42) peptide self-aggregation: elucidation of inhibitors' mechanism of action. ChemBioChem. 8 (2007) 2152-2161.

[43] Z. Sang, X. Qiang, Y. Li, R. Xu, Z. Cao, Q. Song, T. Wang, X. Zhang, H. Liu, Z. Tan, Y. Deng, Design, synthesis and evaluation of scutellarein-O-acetamido alkylbenzylamines as potential multifunctional agents for the treatment of Alzheimer's disease. Eur. J. Med. Chem. 135 (2017) 307-323.

[44] L. Di, E.H. Kerns, K. Fan, O.J. McConnell, G.T. Carter, High throughput artificial membrane

permeability assay for blood-brain barrier. Eur. J. Med. Chem. 38 (2003) 223-232.

[45] Z. Cao, J. Yang, R. Xu, Q. Song, X. Zhang, H. Liu, X. Qiang, Y. Li, Z. Tan, Y. Deng, Design, synthesis and evaluation of 4'-OH-flurbiprofen-chalcone hybrids as potential multifunctional agents for Alzheimer's disease treatment. Bioorg. Med. Chem. 26 (2018) 1102-1115.

[46] J.Y. Kim, H. J. Lim, J. S. Kim, D. H. Kim, H. J. Lee, H. D. Kim, R. Jeon, J.H. Ryu, In vitro anti-inflammatory activity of lignans isolated from Magnolia fargesii. Bioorg. Med. Chem. Lett. 19 (2009) 937-940.

[47] Y.X. Yang, L.T. Zheng, J.J. Shi, B. Gao, Y.K. Chen, H.C. Yang, H.L. Chen, Y.C. Li, X.C. Zhen, Synthesis of 5α-cholestan-6-one derivatives and their inhibitory activities of NO production in activated microglia: discovery of a novel neuroinflammation inhibitor. Bioorg. Med. Chem. Lett. 24 (2014) 1222-1227.

[48] G.K. Hagos, S.O. Abdul-Hay, J. Sohn, P.D. Edirisinghe, R.E.P. Chandrasena, Z. Wang, Q. Li, G.R. Thatcher, Anti-inflammatory, antiproliferative, and cytoprotective activity of NO chimera nitrates of use in cancer chemoprevention. Mol. Pharmacol. 74 (2008) 1381-1391.

[49] N. Cesari, C. Biancalani, C. Vergelli, V. Dal Piaz, A. Graziano, P. Biagini, C. Ghelardini, N. Galeotti, M.P. Giovannoni, Arylpiperazinylalkylpyridazinones and analogues as potent and orally active antinociceptive agents: synthesis and studies on mechanism of action. J. Med. Chem. 49 (2006) 7826-7835.

Graphical abstract

AChE inhibition activity
*Rat*AChE IC$_{50}$: 10.4 μM
*Ee*AChE IC$_{50}$: 15.2 μM

Inhibition Aβ1-42 aggregation
Self-induced: 42.5% at 25.0 μM
Cu^{2+}-induced: 31.4% at 25.0 μM

Antioxidant activity
2.46 Trolox equivalents

BBB permeability

15b

Biometal chelating abilities
Anti-neuroinflammatory ability

Disaggregation Aβ1-42 aggregation
Self-induced: 23.4% at 25.0 μM
Cu^{2+}-induced: 27.0% at 25.0 μM

Highlights

- Novel salicylamide derivatives were synthesized.

- Most compounds showed selective AChE inhibitory and significant antioxidant activities.

- Some compounds exhibited good inhibition of self- or Cu^{2+}-induced Aβ aggregation.

- Some compounds exhibited moderate effect on the disaggregation of Aβ aggregation.

- Compound **15b** showed good anti-neuroinflammation activity and BBB permeability.